CHALMERS

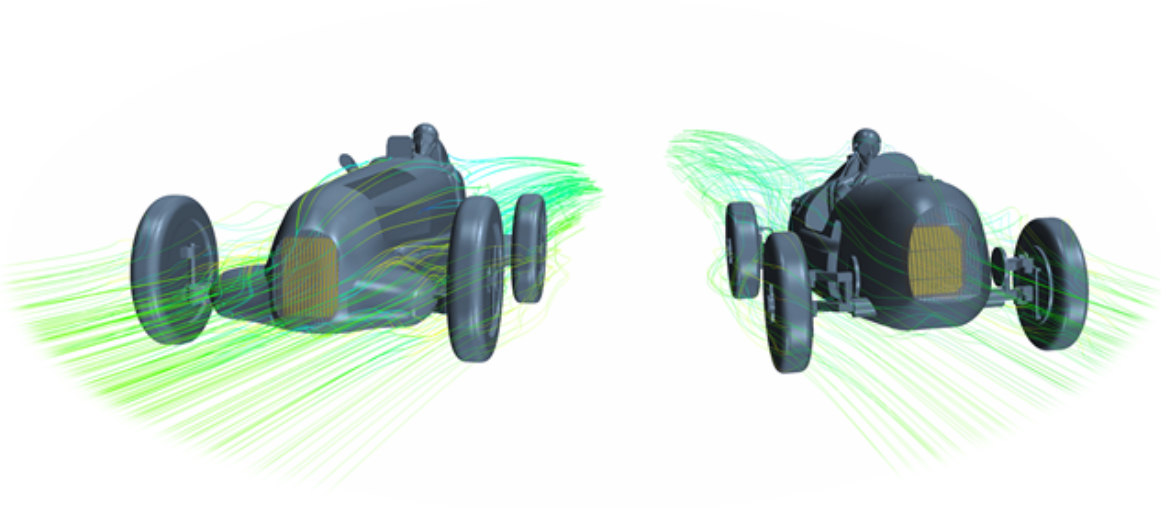

A CFD Analysis and Aerodynamic Comparison of Two Silver Arrows

Bachelor Thesis in Applied Mechanics

FREDRIK EJRESJÖ
BJÖRN KANGE
DAVID KJELLSTRÖM
MATHIAS LINDBÄCK
STEFAN LUNDELL
MARKUS MYBECK

Department of Applied Mechanics
Division of Vehicle Engineering and Autonomous Systems
CHALMERS UNIVERSITY OF TECHNOLOGY
Göteborg, Sweden, 2013
Bachelor Thesis 2013:10

BACHELOR THESIS 2013:10

A CFD-analysis and aerodynamic comparison of two Silver Arrows

Bachelor Thesis in Applied Mechanics

FREDRIK EJRESJÖ
BJÖRN KANGE
DAVID KJELLSTRÖM
MATHIAS LINDBÄCK
STEFAN LUNDELL
MARKUS MYBECK

Department of Applied Mechanics
Division of Vehicle Engineering and Autonomous Systems
CHALMERS UNIVERSITY OF TECHNOLOGY
Göteborg, Sweden 2013

A CFD-analysis and aerodynamic comparison of two Silver Arrows
Bachelor Thesis in Applied Mechanics

FREDRIK EJRESJÖ
BJÖRN KANGE
DAVID KJELLSTRÖM
MATHIAS LINDBÄCK
STEFAN LUNDELL
MARKUS MYBECK

Bachelor thesis 2013:10
ISSN 1654-4676
Division of Vehicle Engineering and Autonomous Systems
Chalmers University of Technology
SE-412 96 Göteborg
Sweden
Telefon: + 46 (0)31-772 1000

Cover: Velocity streamlines around two Silver Arrows

Department of Applied Mechanic
Göteborg, Sweden 2013

Abstract

During 1933 to 1939 the sport of racing was completely dominated by the German manufactures Auto Union (known today as Audi) and Mercedes-Benz. With their superior race cars (named Silver Arrows after their shining bodies and blistering acceleration) the German racing teams were victorious in most of the Grand-Prix races during this period. The cutting edge technologies in these cars remain a source of inspiration for new Mercedes-Benz and Audi cars to this day.

The body shape of the Silver Arrows reveal that a great deal of time was spent optimizing the cars from an aerodynamic point of view, with the purpose of minimizing flow resistance. However, the term “downforce”, which is central to design of modern race cars, was relatively unknown. Compared to the modern use of powerful computers, the possibility of making flow calculations was also very limited at the time.

In this project, two Silver Arrows (Auto Union Type C and Mercedes-Benz W25) have been analyzed from an aerodynamic point of view with the main purpose of calculating lift and drag force. No CAD-data was available for the cars which is why they have been modeled from scratch. Two CMC-models of the cars, scaled 1:18 were used as a baseline. These were laser scanned at Volvo Cars. Curves for both cars have been extracted from the scanned data. With the profile curves as support, the bodies of the cars were modeled in CATIA V5 and from separate measurements the details of the cars were modeled. The final CAD-models were transferred to ANSA where initial surface meshes were generated.

In STAR CCM+ high quality CFD-compatible surface meshes were generated. Volume meshes were then constructed and used in the simulations. The simulations were run with the boundary conditions rotating wheels and a moving ground at 80km/h. Pitch and yaw angels were set to 0^0. The results of the simulation were analyzed and visualized using the post processing tools in STAR CCM+.

The results of the simulations show that the Silver Arrows have good basic shapes from an aerodynamic perspective, but their design also include several drag-producing features and details. Both cars have little to no downforce, which was expected due to the lack of knowledge about the phenomenon at the time.

Overall, the group is content with the result of the project and considers the objectives to be fulfilled. However, because of the emphasis on the pre processing, some planned parts needed to be excluded from the project. Originally, CFD-simulations were supposed to be performed in two different velocities. Also, wind tunnel testing of the CMC-models was to be carried out, and the obtained results were to be compared with the simulations. These parts would have contributed to a more thorough analysis of the Silver Arrows, why the project group recommends further tests and simulations.

Sammanfattning

Mellan åren 1933 och 1939 dominerades racingsporten av de tyska biltillverkarna Auto Union (idag Audi) och Mercedes-Benz. Med sina överlägset kraftfulla tävlingsbilar (med smeknamnet Silverpilar efter sina glänsande chassin och mäktiga acceleration) segrade de tyska racingstallen i merparten Grand-Prix-tävlingar under denna period. Den banbrytande tekniken bakom dessa bilar är än idag en inspirationskälla för nya Mercedes-Benz- och Audi-modeller.

Bilarnas chassiutformning avslöjar att mycket vikt vid utvecklingsarbetet lades på optimering ur ett aerodynamiskt perspektiv med syfte att minska strömningsmotståndet. Däremot var begreppet ”downforce” (nedåtriktad kraft som ger ökat väggrepp) som är centralt vid design av tävlingsbilar idag relativt okänt för dåtidens forskare. I jämförelse med dagens verktygslåda var dessutom tekniken för strömningsanalys överlag betydligt mer begränsad.

I detta projekt har två Silverpilar (Auto Unions Type C och Mercedes-Benz W25) analyserats ur ett aerodynamiskt perspektiv. Någon tidigare CAD-data för bilarna finns ej, därför har dessa modellerats från grunden. Till förfogande har gruppen haft två CMC-modeller av bilarna, skala 1:18. Dessa har laserscannats vid Volvo Cars och utifrån scannad data har profilkurvor för respektive bil tagits fram med hjälp av ANSA. Med stöd av profilkurvorna har bilkropparna modellerats i CATIA V5 och utifrån mätdata från modellerna har separata bildelar ritats. De färdiga CAD-modellerna importerades sedan i ANSA där ett ytnät genererades.

I STAR CCM+ skapades CFD-kompatibla volymsnät av hög kvalitet som sedan användes i simuleringarna. Bilarnas aerodynamiska prestanda undersöktes för hastigheten 80 km/h. Randvillkoren för simuleringarna var roterande hjul och rullande golv, pitch- och yaw-vinklarna sattes till 0^0.

Resultatet av simuleringarna visar att Silverpilarna hade en bra grundform ur ett aerodynamiskt perspektiv men att deras design även inkluderar flera detaljer som producerar luftmotstånd. Bilarna uppvisar ingen eller liten downforce vilket var väntat med tanke på bristen av kunskap om ämnet vid den aktuella tiden.

Överlag är gruppen nöjd med resultatet av projektet och anser att målen är uppfyllda. Däremot kom mycket av arbetet att fokusera på ”pre-processing”-fasen, vilket har gjorde att några planerade delar fick strykas ur projektet. CFD-simuleringarna skulle gjorts vid två hastigheter och vindtunneltester var planerat för att kunna jämföra resultaten. Dessa delar hade bidragit till en bredare analys av Silverpilarna och gruppen rekommenderar vidare tester och analyser.

Nomenclature

Aerodynamic drag	Force that resisting the forward motion of the vehicle
Aerodynamic lift	Force acting vertical to the vehicle
ANSA	A computer-aided engineering program
CAD	Computer-Aided Design
CFD	Computational Fluid Dynamics
CMC	Classic Model Cars, manufacturers of model cars
Downforce	A force acting downwards as a negative lift force
Newtonian fluid	A fluid that follows the relation $\tau = \mu \frac{du}{dy}$
PID	Part Identification
Pitch angle	The angle between the car´s longitudinal axis and the horizontal plane
RANS	Reynolds Averaged Navier-Stokes equation
Yaw angle direction	The angle between the car longitudinal axis and the relative wind
a	Speed of sound
A	Projected frontal area
A_0	Constant
A_S	Constant
B	Fluid property
C_D	Drag coefficient
C_p	Pressure coefficient
C_μ	Turbulence model constant
f_r	Rolling resistance coefficient
F	Force
FL_{Front}	Lift forces at the front axis
FL_{Rear}	Lift forces at the rear axis
g	Gravity
k	Specific-heat ratio
L	Length
m	Mass

M_{Rear}	Momentum around the rear axis
Ma	Mach number
n	Outward normal unit vector
N	Normal force
p_∞	Free stream static pressure
P	Static pressure
P_0	Stagnation pressure
R	Gas constant
R_e	Reynolds number
$\boldsymbol{S}_M$	Body forces
T	Temperature
u^*	Friction velocity
V	Velocity
V_∞	Free-stream speed
y^+	Distance normal to the surface
β	$\frac{dB}{dm}$
ε	Dissipation
θ	Angle
μ	Viscosity
μ_t	Turbulent viscosity
$\boldsymbol{\nu}$	Kinematic viscosity
ρ	Density
τ	Viscous stress
τ_W	Wall shear stress

Preface

This report presents the final results of a bachelor's thesis conducted at the Department of Applied Mechanics at Chalmers University of Technology, Gothenburg, Sweden. The main objective of the project was to construct two CAD-models of the Auto Union Type C and the Mercedes-Benz W25 and perform an aerodynamic analysis of these models. Using the commercial CFD-software STAR CCM+, the analysis was carried out. The project was performed during the period 22/1-22/5 2013.

It is recommended that the reader of this thesis has basic knowledge of the principles of fluid dynamics.

Acknowledgments

We would like to thank Professor Lennart Löfdahl for the opportunity to work with this interesting project and for his helpful guidance throughout the work process.

Also, a great thanks to our supervisors, Ph.D students Alexey Vdovin and Teddy Hobeika, for their patient assistance throughout all steps of the project, and to the people at Volvo Cars how provided the laser scanned data.

Table of Contents

1 Introduction

In this section the background and the purpose of this project is explained and a brief introduction to the development of the Silver Arrows is presented.

1.1 Aerodynamics of the Silver Arrows

Between 1934 and 1939 the sport of racing was completely dominated by the Silver Arrows – a series of cars manufactured by Mercedes-Benz and Auto Union (the latter is known today as Audi). These cars, the fastest race cars the world had yet seen, were equipped with state of the art technology that lacked other comparison, and are still a source of inspiration in design of new Audis and Mercedes-Benz. The cars were used in both Grand-Prix races (a predecessor of today's Formula-1 competitions where world class drivers competed for titles) and also in different forms of high-speed record attempts.

Racing was at this time associated with great risks - many fatal accidents occurred during the Grand-Prix competitions. To increase the drivers' safety, new rules limiting the weight of the cars to only 750 kg (excluding driver, fuel, oils, coolant and tires) were introduced in 1934. In order to meet the weight criteria, designers had to resort to lighter engines. This fact made aerodynamic performance more vital, since cars with a good design in terms of aerodynamic capacity could reach great speeds despite of their weaker engine. Aerodynamics was at this time a rather unexplored area of research, no proper tools for aerodynamic analysis existed. Instead, designers used a more empirical approach to reduce flow resistance. Full-scale models were used in experiments and wind tunnel tests. The final design shows that the developers succeeded with creating shapes that minimizes drag force. (David, 1999)

However, the effect of downforce, which is of great importance in race car design today, was relatively unknown to the developers at that time. By the same principles as the aerodynamic design of a wing makes an airplane lift, downforce is induced by the car's aerodynamic characteristics and increases the traction. This allows greater speeds through corners and improved handling. A few unsuccessful tests with different sorts of diffusers (basically a shape of the underbody that accelerates the flow beneath the car and reduces pressure) were carried out with the Silver Arrows, but lacking proper tools for evaluating and calculating aerodynamic performance, the development came to a rest. (David, 1999)

Today, the technique used in aerodynamic design is much more powerful and well developed. The use of computers and CFD-software is a certainty in most forms of automotive development, but no calculations of the aerodynamic performance of the Silver Arrows have ever been conducted.

1.2 Objective

The objective of this project is to examine the aerodynamic performance of an Auto Union Type C and a Mercedes W25 using commercial CFD-software (STAR CMM+). The result will be analyzed and a comparison of the two vehicles will be performed. A brief comparison of the aerodynamic performance of the race cars' competitors will also be conducted. With the data and analysis of the simulations complete, these following questions will be resolved:

- How good is the aerodynamic performance of the cars regarding lift and drag?
- What are the differences in aerodynamic performance between the cars?
- Are there any weak aerodynamic areas on the cars?

- How does the Silver Arrows' aerodynamic properties compare to their competitors' and more modern vehicles?

Since there exists no previous CAD-data, modeling of CAD-models needed for the CFD-simulations will be made from scratch. Two model cars of scale 1:18, manufactured by CMC, will be used for measurements.

1.3 Delimitations

As the project concerns a quite complex issue, necessary delimitations have been set in order to simplify the problem.

- Only one direction of flow will be considered in the simulations, pitch and yaw angles will be 0°.
- Thermodynamic effects, e.g. generated heat from the engine, will not be considered.
- The external details of the cars will be modeled with some simplification.
- Internal parts will be approximated with low level of detail.
- The flow through the cars will be limited and simplified.
- The wheels of the cars will be modeled with flat sides instead of spokes.
- No acceleration of the car will be considered.
- The number of cells used in the volume meshes was limited to 10-15 millions.
- The project will be carried out during the period 22/1-22/5 2013.

Historical background of the Silver Arrows

This section contains a historical background of the Silver Arrows. A brief description of the development of the cars and story of the name is presented.

A rapid development of race cars took place between the mid 30s and the Second World War. Several prominent automobile manufacturers mainly from Germany, England, France and Italy engaged in the sport of racing, and race car technology became a prestigious field of research. The French racing teams, with Bugatti first in line, were dominant until the late 20s when Italy's Alfa Romeo and Maserati began claiming victories in the Grand-Prix. In 1933 however, both the French and Italians were to see themselves outraced when the spotlights turned to the German manufacturers, Auto Union and Mercedes-Benz. The following 6 years, they were to dominate the sport of racing with their masterful cars, later to be known as the Silver Arrows. In figure 2-1 the Auto Union Type C is shown on the Grand-Prix race tracks. (David, 1999)

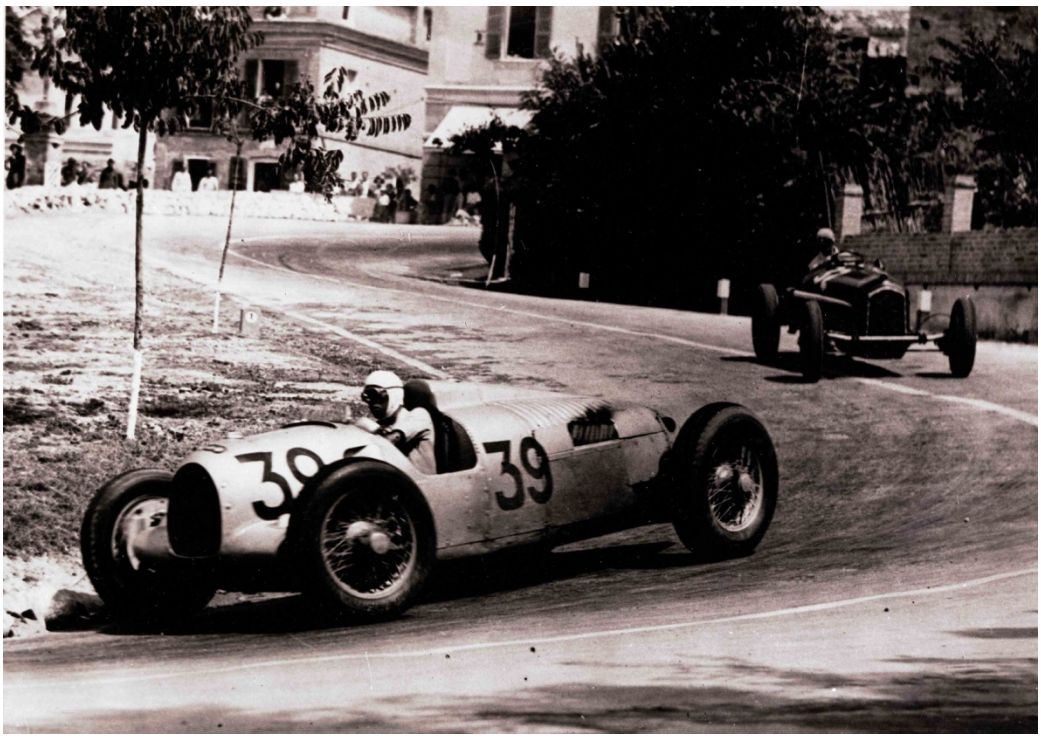

Figure 0-1: The Auto Union Type C in action during a Grand-Prix race. © Audi Photo Archive

1.4 The development of the Silver Arrows

The new rules limiting the weight of the cars to 750 kg forced the designers to create lighter and yet more efficient models, which pushed the development of the race cars even further. The main objective of the new regulation was curbing the speed around the race tracks by pensioning the older generations of powerful race cars. However the development did not turn out as planned, the new models simply turned out to be the starting point of a striving towards even faster vehicles.

During the 30s, the German government made large infrastructural investments with focus on transport, including the Autobahn and the development of the "Peoples car" (Volkswagen Type 1). The racing project was supported as well, government funding was divided between the two competing racing teams in order to support the development of these new high technology racing cars.

The two German manufactures had different technical approaches to their design. The Auto Union was designed by Ferdinand Porsche - an Austrian automotive engineer known today worldwide as the man behind the Volkswagen Type 1 and of course as the founder of Porsche AG. Porsche chose a mid-mounted V16 engine layout which at this time was a very unusual design, but a layout widely used today. However, the geometry of the suspension and the weight distribution resulted in difficult handling, only a handful of drivers could control this powerful vehicle. Figure 2-2 shows a cross section of the C-Type. (Barnard, 2009)

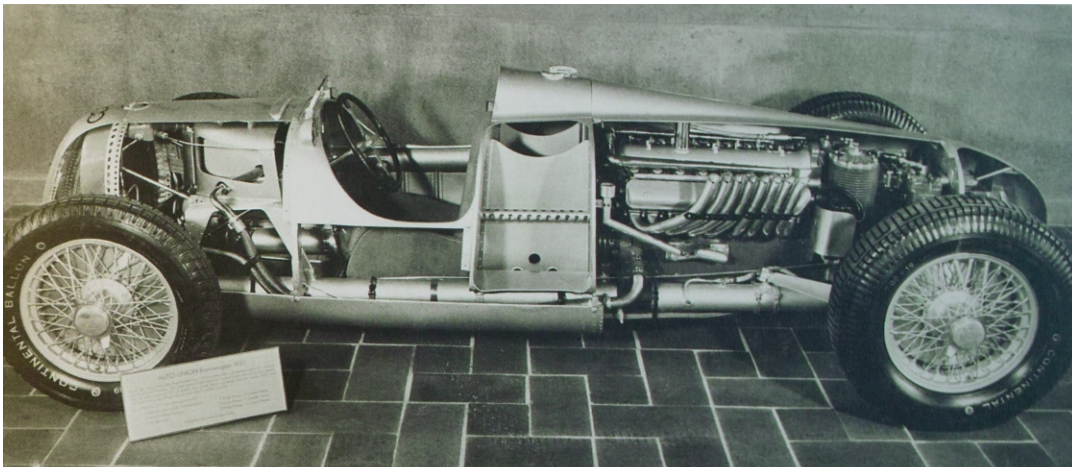

Figure 0-2: Cross section of the C Type. (Kirchberg, 2008)

The Mercedes-Benz on the other hand was based on a more conventional design with a front mounted straight-8 engine. The W25, shown in figure 2-3, was designed by Nibel/Heess and used proven design approaches, though large measures were taken to shed weight such as using a pierced box type chassis and a gearbox made of aluminum. (Snellman, 2012)

Figure 0-3: Mercedes-Benz W25, 1934. © Mercedes-Benz

1.5 The legend of the name

The models became known in the press as the Silver Arrows, referring to their shiny aluminum chassis that, according to some sources, was a consequence of the weight regulations. Normally all the competing cars were painted in accordance with the international racing colors, yellow for Belgium, green for Britain, red for Italy, blue for France and white for Germany. When the new Mercedes-Benz W25 was first launched and scaled prior to the Eifel Grand-Prix at the Nürburgring in 1934, a dry weight of 751 kilograms was noted. In order to meet the new weight criteria the white paint was scratched off the day before the competition revealing the shining aluminum beneath. Silver was later to be adopted as the official racing color by both teams - hence the nickname the “Silver Arrows”. (Becker, 2002)

Regardless of the origin of the name, the dominance of the Silver Arrows cannot be questioned. During 1934-1939 the Grand-Prix races mainly meant battles between the Mercedes and Auto Union drivers. With their tremendous speed and acceleration that far exceeded the capabilities of other competitors these cars entered the racing scene and left the audience in awe. The Silver Arrows were victorious in most of the Grand-Prix races run during these years - only the outbreak of the World War II would end the era of the fastest race cars the world had yet seen.

Basic theory of fluid dynamics

This section will present and discuss the basic principles and laws of fluid dynamics, which the aerodynamic analysis in this report is based on. Methods for calculations and simulations will also be presented.

1.6 Reynolds transportation theorem

The basic laws of mechanics are written for a system that is defined as an arbitrary quantity of mass of fixed identity. In fluid dynamics the mathematics are converted to apply to a specific region rather than for a system. This conversion is called the Reynolds transport theorem and it can describe the basic laws such as the conservation of mass, the angular momentum relation and the linear momentum relation, also called Newton´s second law over a specific region. Reynolds transport theorem can differ slightly depending on if the control volume is moving, fixed or deformable.

Reynolds transport theorem is

$$\frac{d}{dt}\left(\boldsymbol{B_{syst}}\right) = \frac{d}{dt}\left(\int_{CV} \boldsymbol{\beta \rho}\, \boldsymbol{dV} + \int_{CS} \boldsymbol{\beta \rho (V \cdot n) dA} \right) \quad \text{(Eq. 0-1)}$$

B can be any property of the fluid, $\beta = \frac{dB}{dm}$, CV is the control volume and CS is the surface of the control volume, ρ is the density of the fluid, n is the outward normal unit vector in every point on the control surface, V is defined as the velocity (M.White, 2011).

1.7 Incompressible flow

An assumption that the air is incompressible is made, meaning the air density does not change with pressure (Barnard, 2009). This is a generally accepted assumption at Mach numbers under 0.3.

The Ma-number is a dimensionless number based on the relation of the speed (V) and the speed of sound of a perfect gas (a), the relation can be seen in equation 3-2 and 3-3:

$$\boldsymbol{a} = \left(\frac{\boldsymbol{kP}}{\boldsymbol{\rho}}\right)^{\boldsymbol{1/2}} = (\boldsymbol{kRT})^{\boldsymbol{1/2}} \quad \text{(Eq. 0-2)}$$

$$\boldsymbol{Ma} = \frac{\boldsymbol{V}}{\boldsymbol{a}} \quad \text{(Eq. 0-3)}$$

a is the speed of sound in a gas and it is depending on R that is the gas constant, T the temperature in Kelvin, ρ the density, k the specific heat ratio and the pressure P. (M.White, 2011)

1.8 Relation between velocity and pressure

A fluid, in this case air, is affected by an object moving through it. By assuming that the air flow is laminar, frictionless and incompressible it is possible to apply the Bernoulli equation:

$$\boldsymbol{P_1} + \frac{\boldsymbol{1}}{\boldsymbol{2}}\left(\boldsymbol{\rho V_1^2}\right) = \boldsymbol{P_2} + \frac{\boldsymbol{1}}{\boldsymbol{2}}\left(\boldsymbol{\rho V_2^2}\right) = \boldsymbol{constant} \quad \text{(Eq. 0-4)}$$

Bernoulli´s equation is a balance of pressure and kinetic energy. The stagnation pressure P_0 is the highest possible pressure in the flow and is located where the velocity is zero.

The static pressure in the fluid flow are $P_1$and P_2 and $\frac{1}{2}(\rho V^2)$ is the dynamic pressure. This tells us that an increase in local air velocity will decrease the static pressure. However, Bernoulli's equation explains the relation between pressure and velocity in a very simplified way. (Barnard, 2009) (M.White, 2011)

1.9 Traction forces

The force to propel the vehicle is an addition of the tire rolling resistance (F_R), aerodynamic drag (F_D), the force of inertia ($F_{Inertia}$) and the grade (F_{Grade}), as seen in equation 3-5, see also figure 3-1 that shows the forces in a free body diagram (Sovran, 1996).

$$\boldsymbol{F_{Tractive} = F_R + F_D + F_{inertia} + F_{Grade} = Nf_r + \frac{1}{2}\rho V^2 AC_D + M\frac{dv}{dt} + mg\ \sin\theta} \quad \text{(Eq. 0-5)}$$

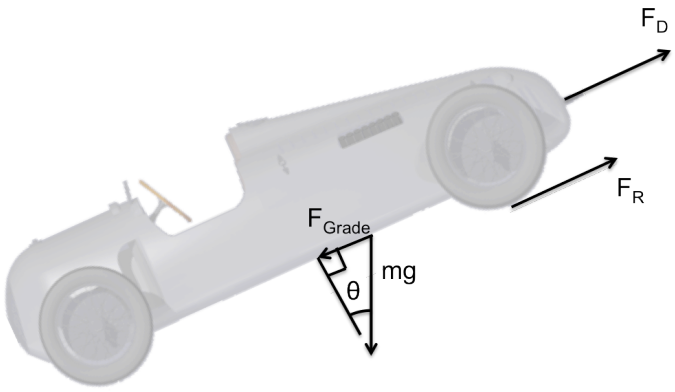

Figure 0-1: Free body diagram

Due to the 0° pitch and yaw angels and the absence of acceleration, the interested forces are therefore the drag force and lift force.

1.10 Aerodynamic forces

The aerodynamic force (F_{Total}) is the resulting vector from the vectors aerodynamic lift (F_{Lift}) and aerodynamic drag F_{Drag} (McBeath, 2008). This relation is illustrated in the figure 3-2 below.

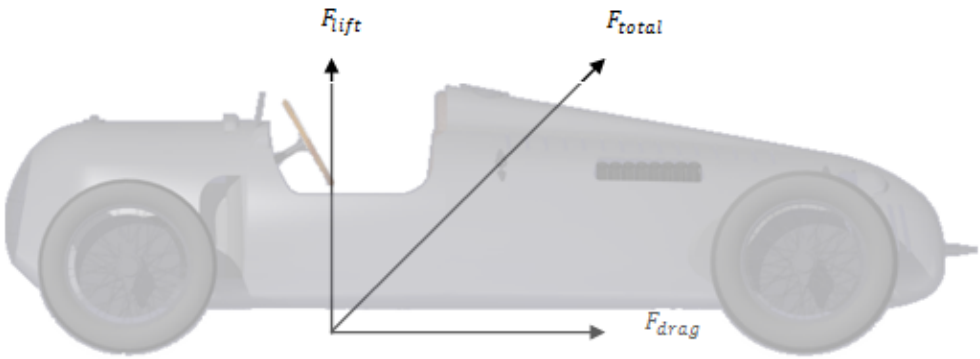

Figure 0-2: Shows F_{total} and its components F_{Drag} and $F_{Lift.}$

Depending on the type of vehicle the forces are different in size and direction. An aircraft is designed so that the lift force is large and cars are usually designed so that the lift force is negative, which is called downforce in this specific case. However, the aerodynamics is very important for the vehicle's handling characteristics and mainly concerns the downforce and the drag force.

1.10.1 Aerodynamic drag

In vehicle aerodynamics it is of great interest to analyze the drag force in order to minimize it. One reason of doing this is that reduced drag has a positive effect on lowering the fuel consumption. There are two main types of drag, the boundary layer normal pressure drag (also known as form drag) and the skin friction drag. The form drag is produced by pressure variations between the front and the rear of the car, meanwhile the skin friction drag is produced due to the viscous effects of the fluid and the surface roughness. For race cars the most significant drag is the one due to pressure variations acting on the car. Because of the separation of flow that are present at the rear, low pressure appears and generates form drag. (McBeath, 2008)

To be able to describe how the pressure varies around the vehicle it is convenient to know the pressure coefficient, C_p , and is defined as the ratio between static pressure and dynamic pressure.

$$\boldsymbol{C_p = \frac{p - p_\infty}{\frac{1}{2}\rho V_\infty^2} = \frac{local\ pressure - (free\ stream\ static\ pressure)}{(free\ stream\ dynamic\ pressure)}} \quad \text{(Eq. 0-6)}$$

Where V_∞ is the driving speed in still air, also called the free-stream speed. The pressure coefficient describes the relative pressure throughout the flow. (Barnard, 2009)

The dimensionless drag coefficient, C_D, gives a good indication on how good the aerodynamic shape of an object is. It is dependent on the shape of the body and the Reynolds number, also a dimensionless number, which is correlating with the viscous behavior of a Newtonian fluid.

Reynolds number:

$$\boldsymbol{R_e = \frac{\rho V L}{\mu} = \frac{V L}{\nu}} \quad \text{(Eq. 0-7)}$$

μ is the viscosity of the fluid, $\frac{\mu}{\rho} = \nu$ is the kinematic viscosity and L is the length of the body.

According to this, the drag coefficient would change with the vehicle speed, but within the range of speed for normal road vehicles C_D can be assumed to be constant. When testing scaled models in wind tunnels the Reynolds number should be taken into consideration. (M.White, 2011) (Barnard, 2009)

The aerodynamic drag is calculated as follows:

$$\boldsymbol{F_{drag} = \frac{1}{2}\rho V^2 A C_D} \quad \text{(Eq. 0-8)}$$

A is the projected frontal area and V is the speed of the vehicle relative to the air and ρ is the density of air (M.White, 2011) (Barnard, 2009).

1.10.2 Aerodynamic lift

By having a lower average pressure on top of the vehicle then on the under body lift force are produced

$$\boldsymbol{F_{lift} = \frac{1}{2}\rho V^2 A C_L} \quad \text{(Eq. 0-9)}$$

for race cars it is desirable to have a negative lift coefficient C_L , which will give a downforce instead of a lift force. This is done to increase the tyre grip and stability of the vehicle (M.White, 2011) (Barnard, 2009).

1.10.3 Force distribution

If the total lift force and the momentum around one of the wheel axis is known, the resulting lift forces at the front and rear axis can be calculated. This will be an indication if the aerodynamics gives the car better grip on the front or the rear axis.

F_{Front} and F_{Rear} are the lift forces at the wheel axis. F_{Lift} is the total lift force. M_{Rear} is the momentum around the rear contact patch and *L* is the wheelbase of the car.

$$\boldsymbol{F_{Front} = \frac{M_{Rear}}{L}} \quad \text{(Eq. 0-10)}$$

$$\boldsymbol{F_{Rear} + F_{Front} = F_{Lift}} \quad \text{(Eq. 0-11)}$$

1.11 Navier-Stokes equations

A partial differential equation, known as the Navier-Stokes equation can be used to describe the dynamics of a fluid. It is a special case of the general continuity equation and is based on the principles of the conservation of mass, conservation of momentum and the conservation of energy.

Some basic assumptions are made in order to derive the Navier-Stokes equations:

- The fluid is seen as a continuum, a continuous substance, rather than a group of discrete particles
- All fields of interest such as density, pressure and velocity are differentiable
- The fluid is a Newtonian fluid
- At low speeds (e.g. Ma < 0.3), fluids can be considered incompressible, thus the viscosity, μ, and the density, ρ, will be seen as constants
- Potential energy is neglected
- The process is at thermodynamic equilibrium, thus the conservation equation of energy is not interesting

The continuity equation shows that the rate of increase of mass in a fluid element equals the net rate of flow of mass into the element:

$$\boldsymbol{\frac{\partial \rho}{\partial t} + \frac{\partial (\rho u)}{\partial x} + \frac{\partial (\rho v)}{\partial y} + \frac{\partial (\rho w)}{\partial z} = 0} \quad \text{(Eq. 0-12)}$$

Assumption of incompressible flow gives:

$$\boldsymbol{\frac{\partial \rho}{\partial t} = 0} \quad \text{(Eq. 0-13)}$$

and hence, the continuity equation:

$$\boldsymbol{\frac{\partial u}{\partial x} + \frac{\partial v}{\partial y} + \frac{\partial w}{\partial z} = div(u) = 0} \quad \text{(Eq. 0-14)}$$

The Navier-Stokes equation can be derived from any of the three conservation equations, through the Reynolds transport theorem. The most elemental form of the Navier-Stokes equation is derived from the momentum equation.

The momentum equation governs on Newtons' second law: "The rate of change of momentum equals sum of forces", including both the body forces and those due to surface stresses. Here, the momentum equation in the x-direction:

$$\boldsymbol{\rho \frac{Du}{Dt} = + \frac{\partial(-p+\tau_{xx})}{\partial x} + \frac{\partial \tau_{yx}}{\partial y} + \frac{\partial \tau_{zx}}{\partial z} + S_{Mx}} \quad \text{(Eq. 0-15)}$$

where $\boldsymbol{S_{Mx}}$ is the body forces.

Also, viscous stresses are needed to be taken in consideration. Here they are expressed as functions of the local deformation rate tensor, with the significant simplification of incompressible flow:

$$\boldsymbol{\tau = \begin{matrix} \tau_{xx} & 0 & 0 \\ 0 & \tau_{yy} & 0 \\ 0 & 0 & \tau_{zz} \end{matrix}} \quad \text{(Eq. 0-16)}$$

Where

$$\boldsymbol{\tau_{xx} = 2\mu \frac{\partial u}{\partial x} - \frac{2}{3}\mu\, div(u)} \quad \text{(Eq. 0-17)}$$

Finally, the momentum equation including the viscous stress terms forms the Navier-Stokes equation:

$$\boldsymbol{\rho\left(\frac{\partial(v)}{\partial t} + v\, div(v)\right) = -\mathbf{div}(p) + \mu\, \mathbf{div}^2(v) + S_M} \quad \text{(Eq. 0-18)}$$

(Batchelor, 2000) (M.White, 2011)

1.12 Turbulence modeling

The flow passing a car acts turbulent with rapid, chaotic variations of pressure and velocity in space and time. This kind of flow is nearly always impossible to compute analytically, why a turbulence model is used to analyze how the flow behaves. There are several different turbulence models available, with different positive and negative properties.

The model chosen for this project is the realizable k – epsilon model, which is an enhancement of the original k - epsilon model and is based on the Reynolds Averaged Navier-Stokes equation, here on called RANS.

The RANS equation is a time-averaged version of the Navier-Stokes equation where an instantaneous quantity is decomposed to its time-averaged and fluctuating terms. The term in the RANS equation describing the turbulent fluctuations is called Reynolds stresses. This is the terms in need of additional modeling to close the RANS equation for solving.

The original k – epsilon model is a so called two equation model, containing two extra transport equations to describe the turbulent flow. One is transporting the turbulent kinetic energy, k, and the other the turbulent dissipation, ε.

With these parameters, according to the Boussinesq's eddy viscosity assumption, the Reynolds stresses can be described in terms of the turbulent viscosity, μ_t:

$$\boldsymbol{\mu_t = \rho C_\mu \frac{k^2}{\varepsilon}} \quad \text{(Eq. 0-19)}$$

Where $C_\mu = 0.09$

The realizable k – epsilon model differs in two important ways from the original k – epsilon. First, it contains an improved formulation of the model constant C_μ in the turbulent viscosity:

$$\boldsymbol{C_\mu = \frac{1}{A_0 + A_S \frac{kU^*}{\varepsilon}}} \quad \text{(Eq. 0-20)}$$

Secondly, it is using a more accurate model equation for the dissipation ε.

Because of these improvements, the realizable k – epsilon model generates more precise results for flows including rotation, separation and recirculation than the original one. It also predicts the spreading rate of both planar and round jets.

Even though it is not the most accurate model available, regarding the field of external road vehicle aerodynamics it is considered accurate enough for these types of simulations.

Relative to more accurate models it demands low amount of computer power. Because of these factors it is widely used within this area of analysis, hence in this project as well. (Batchelor, 2000)

1.13 Wall treatments

Wall treatments are used to obtain the boundary conditions for the continuum equations, this is done closest to the wall. The turbulent boundary layer consists of three regions

- A viscous sub layer
- The overlap layer
- The outer turbulent layer

In the viscous sub layer laminar shear is dominant near the wall and turbulent shear dominates the outer layer. The intermediate layer between the sub layer and the fully developed turbulent layer exists of both laminar and turbulent shear that then switches to fully turbulent in the outer turbulent layer. The turbulence is increasing fast throughout the layers and can be described by the linear viscous relation

$$\boldsymbol{y^+ = \frac{yu^*}{\nu}} \quad \text{(Eq. 0-21)}$$

$$\boldsymbol{u^* = \left(\frac{\tau_W}{\rho}\right)^{1/2}} \quad \text{(Eq. 0-22)}$$

Where y^+ is the dimensionless distance normal to the surface, u^* is the friction velocity,

τ_W is the wall shear stress, ρ is the density, ν is the kinematic viscosity and y the distance from the edge of the surface (M.White, 2011).

There are usually two approaches to model the viscosity-affected region.

The Near-Wall model approach requires a very fine mesh and tries to resolve the gradients in the boundary layer. This consumes a lot of computing power but generates an accurate solution.

The second approach uses semi-empirical functions, so called wall-functions, to bridge the viscosity-affected region to the fully-turbulence region. This way there is no need to modify the turbulence models because of the wall. With this method the region closest to the wall does not need to be fully solved and therefore this method uses less computational power and saves time. The wall-function approach produces a solution with enough accuracy for most applications. With applications were the flow is highly skewed or laminar, the near-wall model approach is preferred.

In this project, none of these properties is expected. The wall-function approach will therefore produce a good enough solution.

There are two common types of wall-functions that can be used, standard and non-equilibrium. These are illustrated in figure 3-3. The non- equilibrium approach includes some effects of pressure gradients and strong non- equilibrium, which makes its applicability somewhat wider than the

standard approach. As long as the flow conditions do not depart too much from the ideal conations, the wall-functions approach gives reasonably accurate solutions. (FLUENT, 2003)

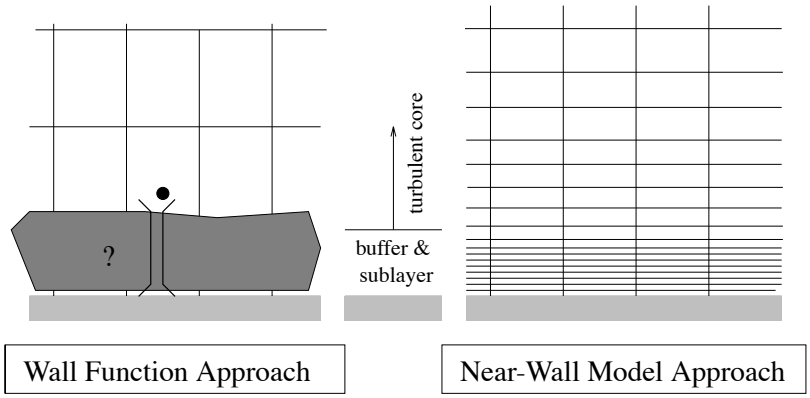

Figure 0-3: Using the Wall Function Approach, the viscosity-affected region is not resolved, instead is bridged by the wall functions. Using the Near-Wall Approach on the other hand, the near-wall region is resolved all the way down to the wall. (FLUENT, 2003)

1.14 CFD and the Finite Volume Method

The equations that represent the physics of fluids are too complex to solve numerically by hand. Therefore Computational Fluid Dynamics, CFD, is used to solve these complicated partial differential equations by the help of computers. There are several different commercial software that can be used to perform CFD-calculations, for example Fluent, COMSOL and Star-CCM+. The mathematical model of the CFD-software is usually based on simplified versions of the Navier-Stokes equations.

To solve these equations, the Finite Volume Method is used. This is a numerical method of solving the partial differential equations describing the fluid flow. The geometrical domain analyzed is divided into a large number of small finite control volumes, called elements or cells, which all together makes a volume mesh. The shapes of the cells are commonly prism with triangular bases, alternatively prism with quadrilateral or polyhedral base.

By applying the finite volume method (FVM) the conservation equations for mass, momentum and energy are integrated over the volume. By interpolation between the center nodes of the cells the equations are solved in each control volume and over the total domain. This is an iterative process that continues until the residuals converge. By using an unstructured mesh, a more complex geometry can be used with good mesh quality still preserved. This makes it possible to have a dense mesh where flow speed changes rapidly, for instance, in turbulent areas where separation occurs and a coarse mesh in more stable flow.

Close to the wall, prism layers are used to capture the boundary layer physics. The prism layer consists of dense prisms that are extrapolated from the surface. (Hansen, 2005) (Finite Volume, 2012)

Method

In this section the general work process of the project and the method used to perform the aerodynamic analysis of the cars will be explained. Selected software and setups used for simulations will be motivated.

To be able to make a proper comparison of the aerodynamic properties of both cars, an aerodynamic analysis had to be carried out. This can be done using several different commercial CFD-software. In this project using STAR CCM+ was beneficial since the software was provided by the institution and the group's supervisors were well familiar with this specific software. The CFD-process was divided into three phases: pre-processing, solving and post-processing. Figure 4-1 summarizes the key points of the different steps in the process.

.

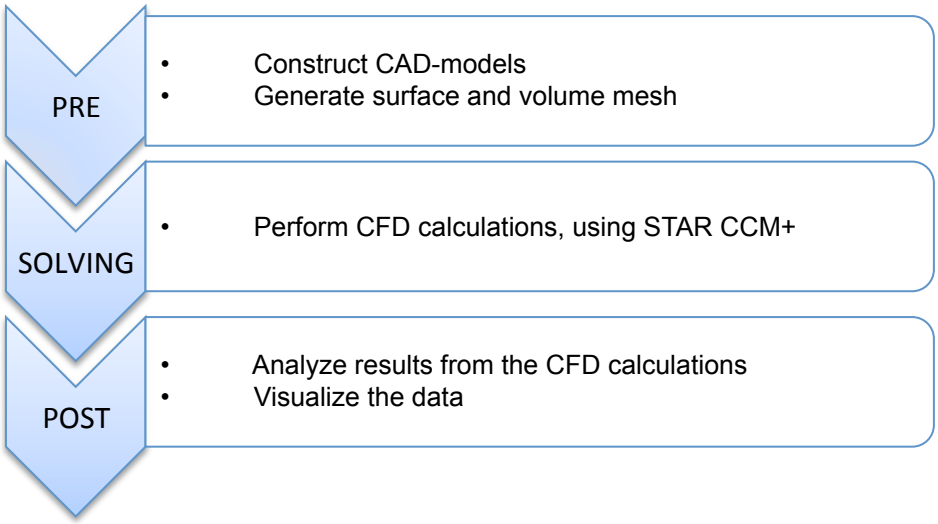

Figure 4-1: Overview of the steps of the CFD-process

Since the group was short of expertise in this type of modeling, a great part of the project concerned gaining knowledge of necessary software and methods to be used. To be able to perform the required actions, tutorials and guides of CATIA, ANSA and STAR CCM+ were studied.

1.15 Pre-processing

The main objective during the pre-processing was creating a good surface and volume mesh of each car to be used in the solving phase. Since no previous CAD-data of the Silver Arrows existed, the first step was to generate two detailed CAD-models of the cars. The group members were most familiar with CATIA V5, hence this software was used for the CAD-related work.

The project's starting point was laser scans of the two CMC-models of the cars. The models are shown in figure 4-2. The scanning had been performed at Volvo Cars and was provided as a format which could be imported to and viewed in ANSA. The scans were of rather poor quality and had to be "cleaned", meaning that unwanted data had to be deleted, before the results could be evaluated. The scans gave a good representation of the general outlines of the cars but required a great deal of reconstruction and furthermore manual modeling of external parts because of imperfections and low level of detail. In other words, a lot of CAD-work was needed to create functional models that would generate good results in the solving phase.

Figure 4-2: CMC-models of the two cars scaled 1:18, the Auto Union to the left and the Mercedes to the right.

1.15.1 External parts

First of all, the external parts were modeled. Which details that needed to be modeled manually was decided by studying the scans. For example the wheels, windshield and exhaust pipes were impossible to recreate using the scans, and so had to be built from scratch using manual measuring from the CMC-models. Since the project had a quite limited time budget not every nut and bolt could be modeled. Details that were not considered to make a substantial impact on the aerodynamic performance, or not characterizing for the design of the cars, were left out of the models. Figure 4-3 shows some of the parts that were modeled manually. All external parts that were modeled can be found in appendix A.

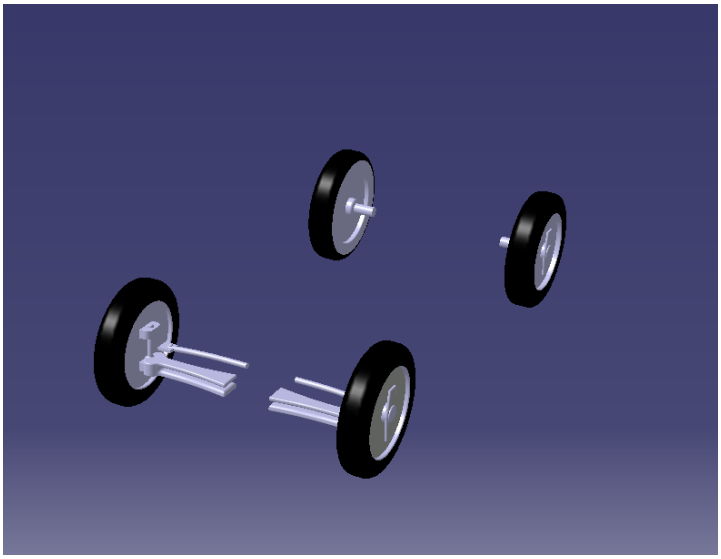

Figure 4-3: Some external parts were modeled manually, for example wheels and the suspensions.

1.15.2 Modeling of the bodies

The next step after finishing the external parts was to create the bodies of the cars. Profile curves of the chassis' shapes could be extracted by manipulating the scans in ANSA. The same basic technique was used to create the body of the Mercedes and the Auto Union. Given that the top and bottom of the cars had been scanned separately, the first task was to fit these parts together.

With the top and bottom properly connected the desired curves could be generated. Figure 4-4 shows the Mercedes-Benz scan with top and bottom connected. Note that the general shape of the cars is well preserved while almost all details are missing.

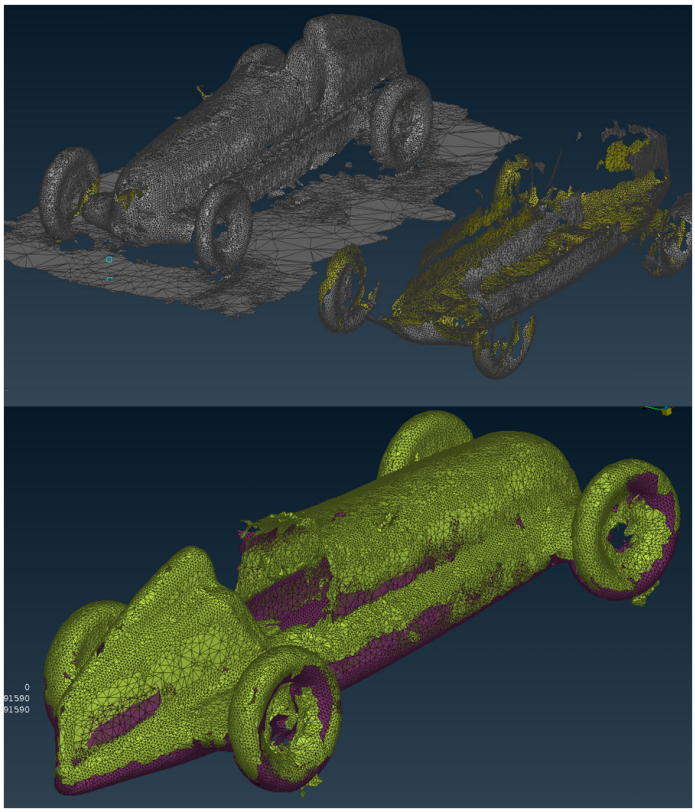

Figure 4-4: Top: Original scans of top and bottom. Bottom: Joint scans of the Mercedes-Benz visualized in ANSA.

By creating vertical planes with regular intervals in the scan-files and performing cuts along these planes, supporting curves for the chassis modeling were extracted. These curves were exported to CATIA and a wireframe of splines was created. By using the “Multi-section surfaces” command in the CATIA wireframe workbench, a surface of the chassis could be created. After some manual adjustments, the CAD-models were imported back into ANSA and compared with the original scans in order to evaluate the created shapes. After reaching the desired result, chassis details and openings were made. Figure 4-5 shows the resulting surface of the Mercedes.

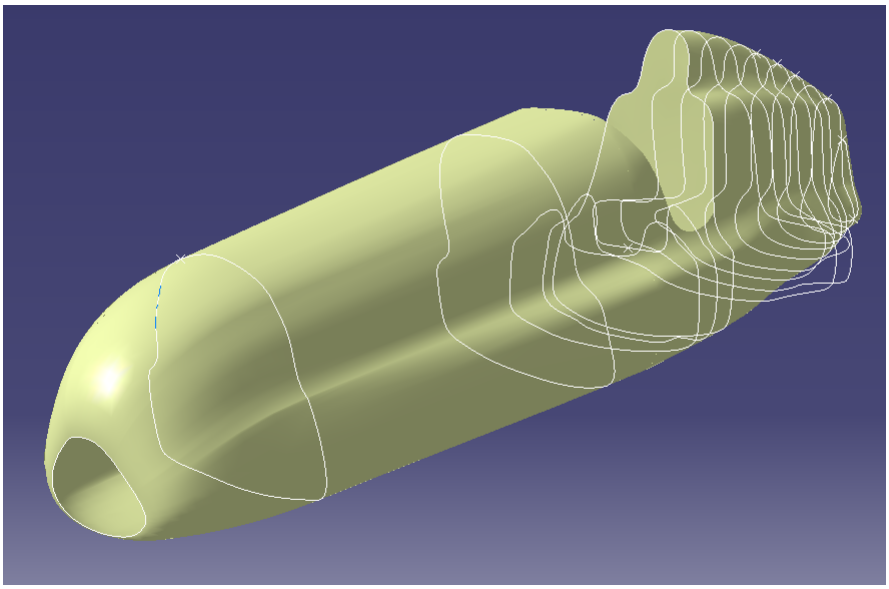

Figure 4-5: Surface of the Mercedes chassis modeled in CATIA, using curves extracted from the scan.

1.15.3 Modeling of the interior

Both original cars are designed to take in rather large volumes of air through the bodies, which is used for cooling of the engine and the cockpit. This causes a complex flow and leads to an even more demanding analysis. In order to simplify the upcoming simulations, the flow through the vehicles was regulated. Some volumes were “sealed off” meaning that the flow was controlled by adding planes to the interior that prevents air from entering these volumes. Since the flow was to be restricted, there was no need for a high level of detail of internal parts.

Figure 4-6 illustrates how the air is supposed to flow through the Auto Union. Air enters through the grill, passes the radiator and exits through the outlets on the sides. On the original car, air can also enter the cockpit from the front, but this passage was closed on the CAD-model. Air can also enter through the rear inlets, but as shown in the figure, the engine bay was sealed off as well.

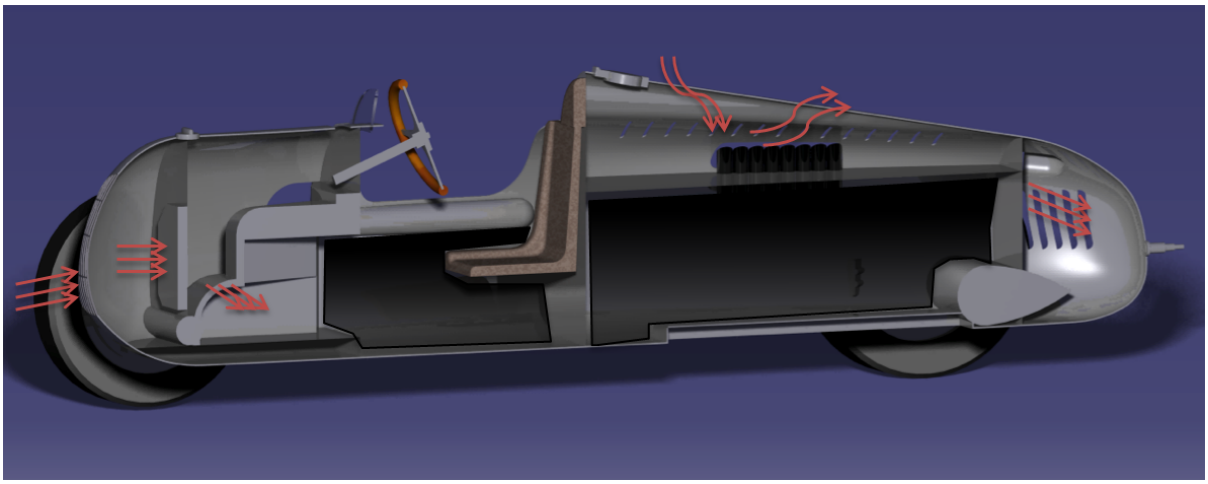

Figure 4-6: The red arrows illustrate the flow path through the interior. Black regions marks volumes were no air flows. Air enters through the grill, passes the radiator and exits on the sides. No air enters the cockpit from the front. Air also enters through the rear inlets, but the engine bay has been sealed off.

On the Mercedes, air only flows through the front parts of the chassis, shown I figure 4-7. The engine was simply approximated by a block. The original car has an air inlet located next to the driver which directs the flow into the cockpit. On the CAD-model, this inlet was closed.

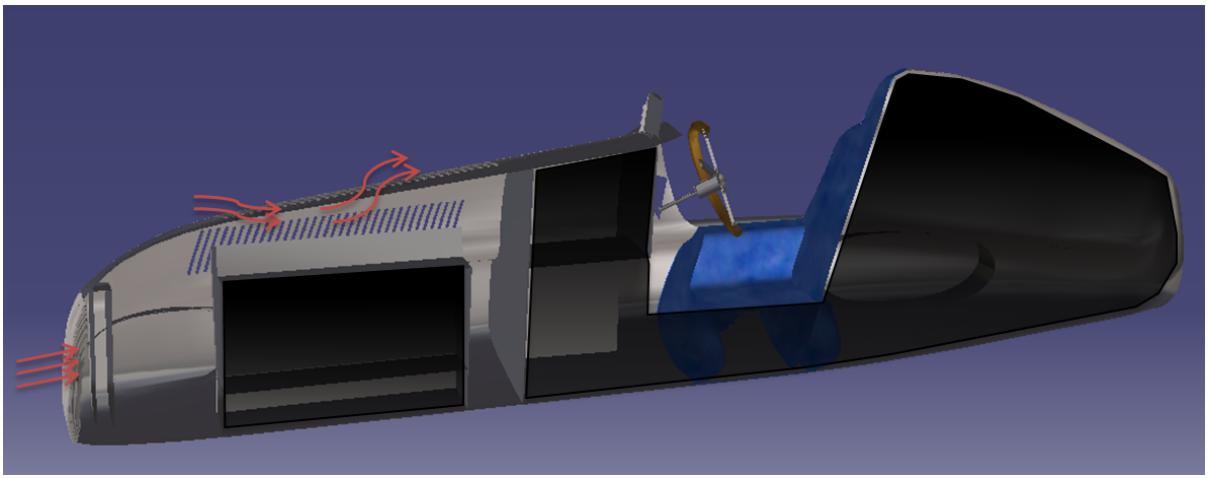

Figure 4-7: Air enters through the grill and passes the radiator. The engine has been approximated by a block. Air also enters and exits through the inlets on the hood. The cockpit and the rear have been sealed off.

1.15.4 Assembling

With all external parts done and the body finished the models were assembled in CATIA. Since only the surfaces were of importance in the upcoming simulations, no effort was made to create constraints to avoid intersecting surfaces. The final CAD-models are shown in figure 4-8.

A human model was then inserted from the CATIA library to represent the driver in the CFD-simulations. To give an authentic feel, a helmet of appropriate design was modeled and fit to the driver. The complete CAD-models including drivers, were then imported to ANSA for preparation and generation of surface meshes. Before proceeding with the processing in ANSA the models were cleaned from unnecessary remains from the assembly and some final adjustments of the shapes were made.

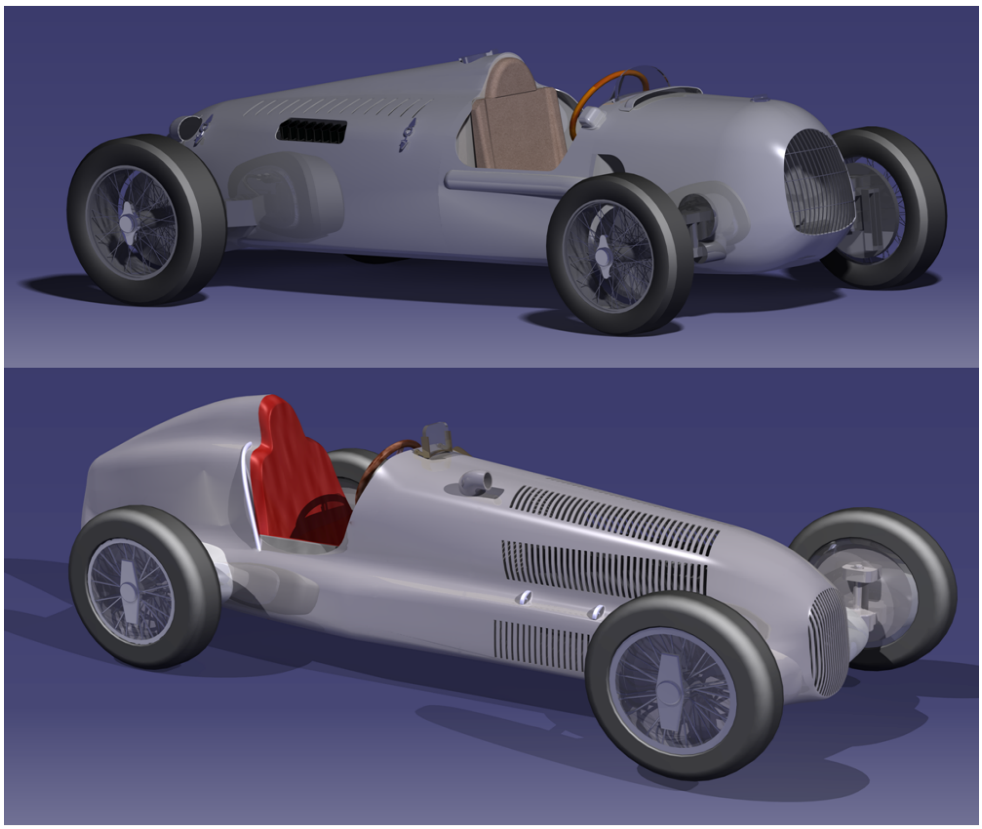

Figure 4-8: Resulting CAD-models of both cars. Top: Auto Union, bottom: Mercedes.

1.15.5 Preparing for an optimal mesh

To save computational power it is always of high importance to avoid wasting cells by using too fine mesh where it is not needed. Since flow around the car body will be affected differently by shapes and openings, a mesh with varying cell-size is desirable. In regions with details or shapes that strongly affect the flow, a fine mesh is needed to provide good results, whereas in regions where the flow is relatively unswayed, a coarser mesh can be used. By assigning parts and regions of different criticality from this perspective to different groups (called PID:s in ANSA) the mesh-size can be controlled in the solving phase. Before mesh-generation in ANSA, which parts and regions that were to be assigned to different PID:s, was decided. The final division of PID:s for the Auto Union is shown in figure 4-9. Parts with similar level of detail were grouped together, settings can be seen in appendix B.

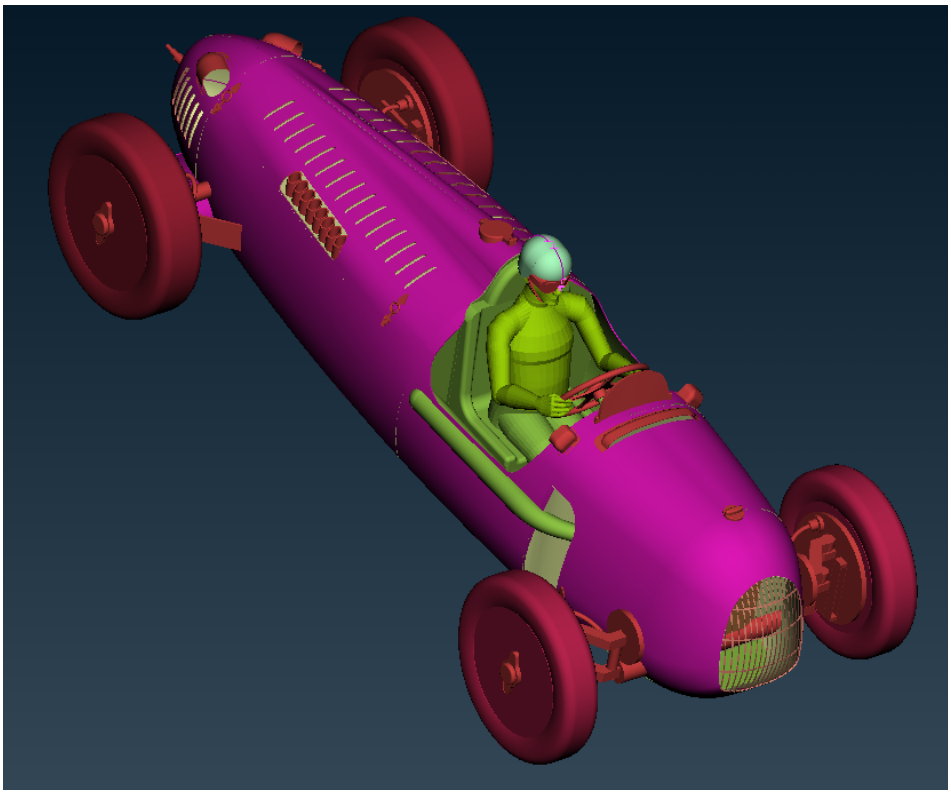

Figure 4-9: Auto Union with different PID:s shown by color.

1.15.6 Creating the volume mesh

With all necessary parts set to different PID:s the models had to be converted to a format readable by STAR CCM+. This was done by meshing the models in ANSA. The surface mesh was then exported to STAR CCM+.

To create a CFD-compatible mesh of high quality, several actions were performed in STAR CCM+. The surface mesh, generated in ANSA, might contain some defects such as holes, overlapping edges and non-manifold surfaces. This can lead to problems during the volume mesh generation in the solving phase. The “Surface Wrapper” is a tool in STAR CCM+ which solves this problem by creating a continuous, “air tight”, surface. This function searches for all surfaces that will be in contact with the outside air and creates a new surface from this data. Gaps and holes, of bigger size than a reference value set by the user, will be patched together.

The surface is then reconstructed. By using the PID:s, different levels of cell sizes (target sizes) were set with smaller values for more complex regions. Finally, STAR CCM+ uses this surface mesh to grow the volume mesh.

Before generating the volume mesh, settings for controlling the cell size needed to be set. As previously mentioned, in order to avoid using an unnecessary large amount of cells, it is desirable to use a finer mesh in areas were the flow will be strongly affected and a coarser mesh in other regions. The growth of the volume mesh can be controlled in different ways. This is achieved either by setting a general growth rate, meaning that the speed of cell growth is predefined, or by using refinement boxes. A block that encloses the object is then created and a maximum cell size inside the block can be set.

Figure 4-11 shows the final volume mesh of the Mercedes, were “very slow” growth was used and five refinement boxes surrounds the car. The outer box represents the wind tunnel, which serves as the

outer boundary for the volume mesh and decides the absolute maximum cell size of the mesh. Some of the refinement boxes used on the Auto Union are shown in Figure 4-10 The same technique was used for generating the volume mesh of the Auto Union. A total number of about 10 million cells were used for each car.

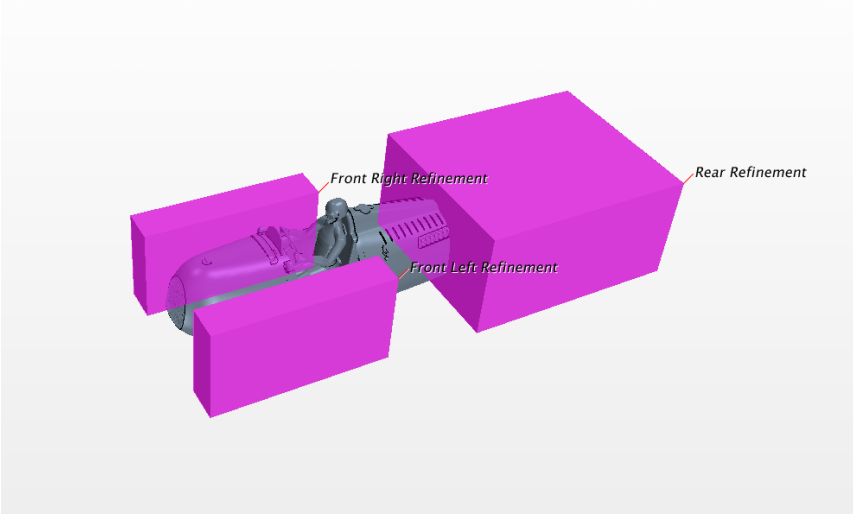

Figure 4-10: Refinement boxes for the Auto Union.

As also can be seen in figure 4-11, a thin layer closest to the surface of the model is built up by a very fine mesh. These are the prism layers (explained in section 3.9.1), which are used to get a good representation of the boundary layer. Three prism layers were used in this project.

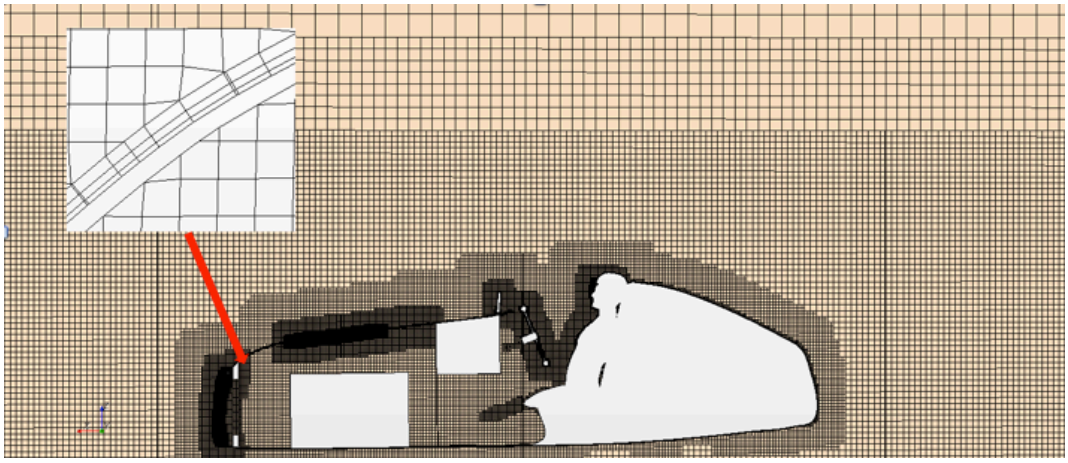

Figure 0-11: Plane cut showing the final volume mesh of the Mercedes, three prism layers has been used. The mesh is finest close to the car. The refinement box and the outer box (the wind tunnel) control the mesh growth.

1.16 Solving

The solving in STAR CCM+ consisted of setting desired values of movement and choosing proper physics models for the simulation. This was done at both a general and more specific level. The velocity, 80 km/h, was set in three places: a moving floor, rotating wheels and an inflow speed set for the air into the wind tunnel. For the wheels the angular velocity had to be calculated, see table 4-1. The flow direction was chosen so that pitch and yaw angles were 0°.

Table 0-1: Angular velocity calculated for the wheels at 80 km/h.

Car	*Front wheels*	*Rear wheels*
Auto Union	58.51 rad/s	55.74 rad/s
Mercedes	56.76 rad/s	54.87 rad/s

The radiator was set as a porous region and resistance values were chosen to simulate a real radiator, see table 4-2. The important values are for the primary direction, the direction of the flow. The values for the secondary direction are set much higher to prevent flow in that direction.

Table 0-2: Resistance values for the radiator, recommended values from STAR tutorial.

Type of resistance	*Primary direction*	*Secondary directions*
Porous Inertial Resistance	90 kg/m^4	90000 kg/m^4
Porous Viscous Resistance	450kg/(m^3*s)	450000 kg/(m^3*s)

Some of the physic settings used in the simulation are listed below:

- Steady state
- 2nd order discretization is used for the coupled flow model
- Two-layer All y+ Wall Treatment
- The realizable K-Epsilon is used as turbulence model
- The default gradient method is used which is “Hybrid LSQ-Gauss”
- Reynolds-Averaged Navier-Stokes
- Initial conditions for the air inlet is set as
    - Velocity=80 km/h
    - Turbulence Intensity=0.01

The coupled flow model solves the conservations for mass and momentum at the same time. The form of the equations that the coupled flow model uses makes it suitable for solving incompressible and isothermal flow.

The 2nd-order discretization is chosen because it gives a better approximation than the 1st-order discretization.

A least square method is implemented to minimize the residuals, to give smaller errors than a linear error-term would result in.

RANS and wall treatments are previously explained. (Section 3.7 and 3.8.)

Turbulence intensity of 0.01 represents that the air in the simulations is motionless unless affected by the cars.

After all values were set the simulation could be started. The results could then be visualized in post processing.

1.17 Post-processing

In post processing the results from the simulations were analyzed using STARCCM+. Several values could be extracted and a large variation of visualizations could be rendered to demonstrate the air behavior in and around the vehicle.

The values extracted from STARCCM+ were drag, downforce, projected frontal area and momentum around the wheel axis. These were used to calculate C_D (eq. 3.8) and the distribution of the downforce (eq. 3.10 and 3.11) between the axis.

Several pictures were chosen to give a good overview of the general airflow as well as a good view of streamlines, pressure areas and velocity fields.

Analysis of the CFD-results

In this section the results from the CFD-calculations will be presented and analyzed. The flow fields will be visualized and the aerodynamic properties of the two cars will be evaluated and compared.

1.18 Aerodynamic properties

Table 5-1 shows the resulting principal aerodynamic properties of the cars, derived from the CFD-calculations. As reference values, C_D and $C_D A$ of the Bugatti type 51 (which was an opponent to Silver Arrows during the Grand-Prix races), as well as of the family car Ford Sierra (1982) have been included. (Barnard, 2009)

Note that both Silver Arrows has a drag coefficient of much smaller value then the Bugatti. The $C_D A$ -factor shows how the design of the Silver Arrows is superior to the Bugatti, in comparison of induced drag force. The Auto Union has a positive lift coefficient which means the aerodynamic forces on the car tries to lift it. The Mercedes-Benz, on the other hand, has a negative lift coefficient that gives the car downforce.

$F_{L\,Front}$ and $F_{L\,Rear}$ is lift forces that act on the cars wheel axis. By studying these forces the cars lift force distribution can be decided. The Mercedes-Benz generates downforce at both the front and rear. The highest downforce occurs over the rear axis. The Auto Union generates a lift force over the rear axis and downforce over the front axis. The aerodynamic lift forces on the cars are rather small compared to other forces on the cars. The lift forces should therefore not affect the cars handling significantly.

Table 5-1: The resulting aerodynamic properties of the Silver Arrows at 80km/h. Values for the Bugatti Type 51 and the family car, Ford Sierra (1985), are used as references.

Model	C_D	$C_D A$	C_L	F_{Drag} [N]	F_{Lift} [N]	$F_{L\,Front}$[N]	$F_{L\,Rear}$[N]
Auto Union Type C	0.60	0.74	-0.01	222.62	-3.50	45.11	-48.66
Mercedes-Benz W25	0.42	0.51	-0.16	151.34	-55.60	-15.94	-39.66
Bugatti Type 51 (1933)	0.74	0.96	-	-	-	-	-
Ford Sierra (1982)	0.34	0.67	-	-	-	-	-

1.19 Flow analysis

Figure 5-1 shows the flow separation for the vehicles, the green regions indicates were separation occurs. Note that the smooth green surface of the front of the Mercedes does not indicate a significant separation. This is merely an effect of the prism layers, the flow is in fact rather well attached to the surface in this region. In general, these results show that the Silver Arrows designers succeeded in creating streamlined shapes. The flow is well attached, meaning that it follows the contours of the chassis well, especially for the Mercedes.

Figure 5-1 also reveals some differences in aerodynamic behavior of the two cars. First of all, the blunt nose of the Auto Union creates a greater separation of flow at the front region, compared to the Mercedes. However, the major differences between the two cars are the mid-regions and the wakes. Note that the separation is more evident in the cockpit region for the Mercedes, whilst the flow reattaches behind the driver of the Auto Union. Thus, the mid-region shape of the Auto Union is more efficient than the Mercedes'.

At the rear, the external features of the Auto Union cause an immense separation of flow, which leads to a vast wake. The rear shape of the Mercedes, on the other hand, enables the flow to reattach to the surface. This pressure recovery region results in a less significant wake, which leads to less drag.

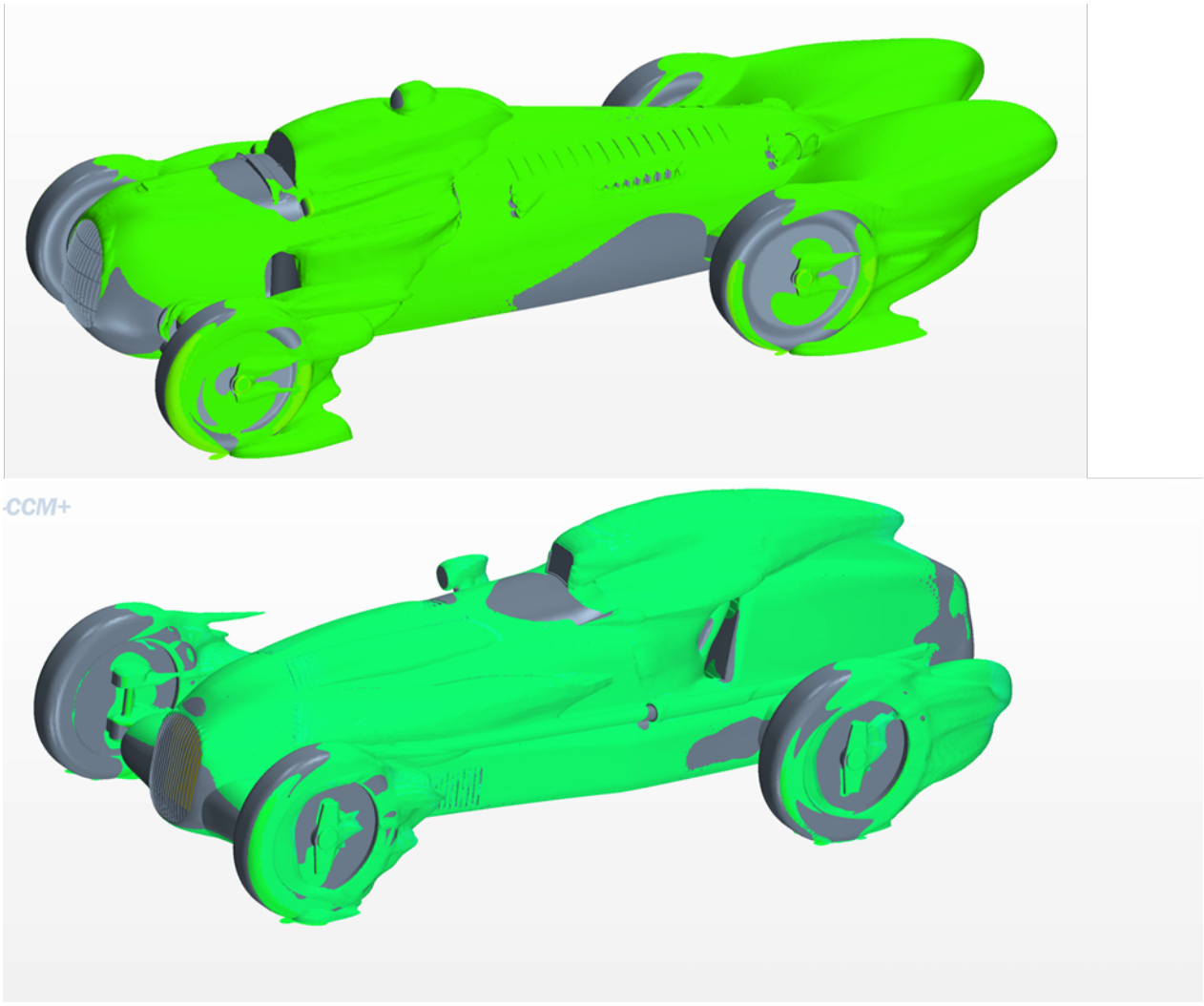

Figure 0-1: Flow separation. The green regions shows areas were the flow separates.

1.20 Drag and lift force induced by the body

As discussed in sec. 3.5, the greatest contribution to the drag force is the boundary layer normal pressure drag, also known as form drag. This drag force component is mainly induced by pressure difference. Since the pressure of the entire internal region is close to stagnation, the resulting net force is zero. Hence, the drag force is decided by the pressure difference of the front and rear. (Barnard, 2009)

Figure 5-2 shows the pressure distribution of both vehicles. Red color indicates pressure of greatest magnitude and blue color indicates low pressure regions. As expected, the pressure is highest at the front, were the flow reaches zero velocity and stagnation pressure is obtained. The pressure is lower in the rear regions, giving rise to a drag force.

Other high pressure regions are tires, suspensions and other external features. The resulting pressure distribution clearly shows that the blunt front shapes and the exposed wheels and suspension could be improved aerodynamically.

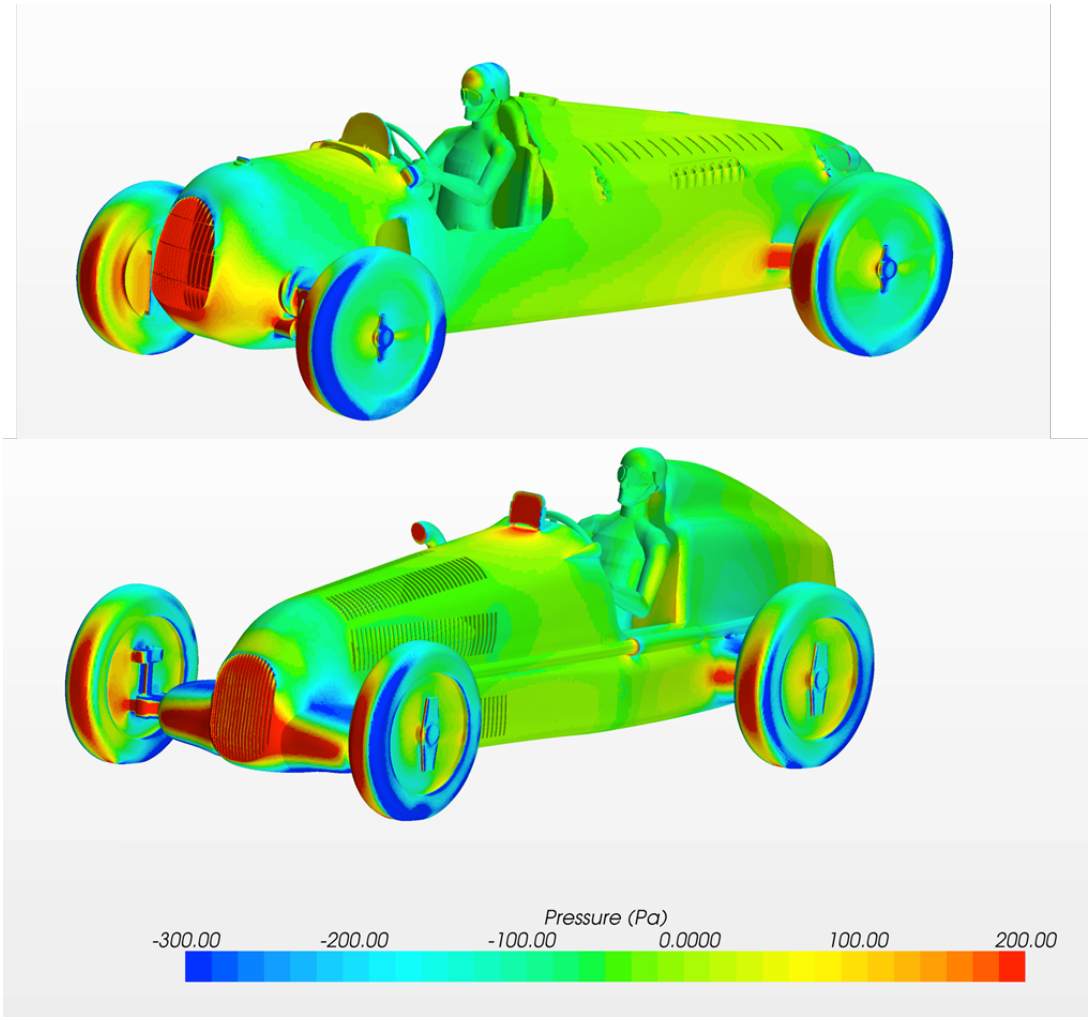

Figure 0-2: Pressure distribution of both vehicles.

As mentioned in section 3.5, downforce is induced in a similar way as drag force. The main factor is the pressure difference between the top and bottom of the vehicle. Hence, to induce downforce, high velocity beneath the car compared to above is desirable. Figure 5-3 shows the scalar velocities of the flow surrounding the cars. Red color indicates flow of greatest magnitude and blue color indicates lower magnitude.

As the figure shows, in both cases, the air flows at higher speeds beneath the car in comparison to the top, hence, creating a downward thrust. Note that for the Mercedes the difference in airspeeds is greatest at the front section, however the numbers presented in table 5-1 shows that the downforce for the Mercedes is greater at the rear. Meanwhile, the magnitude of the downforces is distributed more evenly between front and at the rear for the Auto Union. Figure 5-4 shows the pressure distribution of top and bottom of both cars, which even clearer illustrates the downforces.

This difference in magnitude of the downforce could partly be explained by the difference in ground clearance, which is the distance between ground and body. In principle, a smaller clearance from the ground will cause airflow of higher velocity beneath the car, since the ground limits the area through which the flow can pass this accelerates the flow. This will induce a pressure difference, which generates downforce. As the figure shows, the Mercedes is closer to the ground than the Auto Union.

It is also notable that the flow enters the body and passes the radiator region at rather low speed and decelerates in the engine bay. A rather vast volume of air is recirculating in the internal region which leads to energy losses and also greater drag.

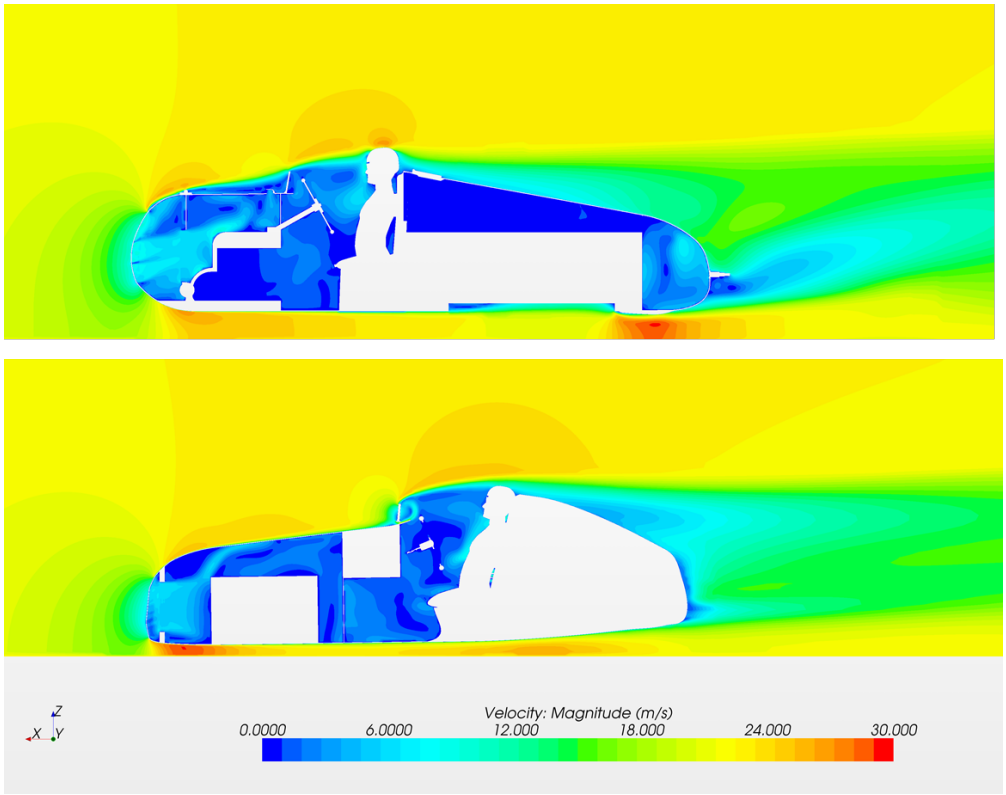

Figure 0-3: Scalar velocities of the flow surrounding the cars. Red regions indicates highest velocities, blue region indicates low velocity regions.

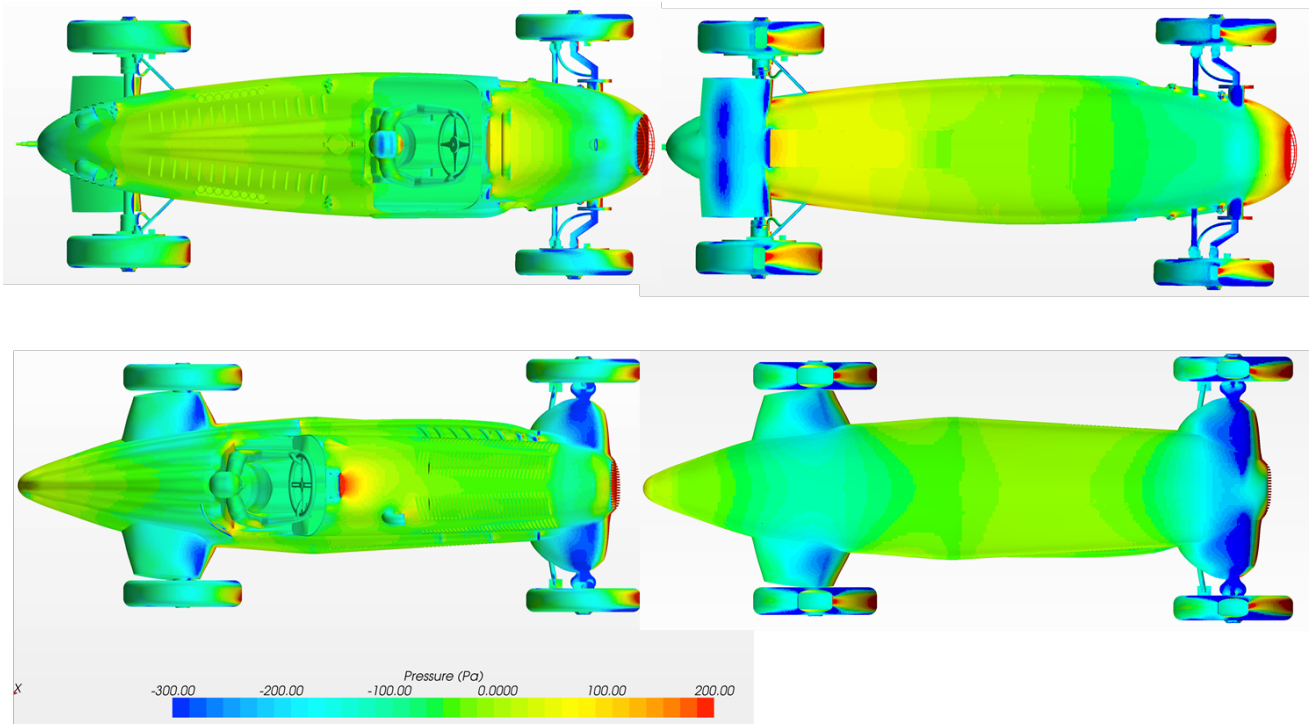

Figure 0-4: Pressure distribution of top and bottom of both cars, shows the distribution of down and lift forces.

1.21 Drag and lift forces induced by the wheels

Figure 5-5 shows the scalar velocities of the flow surrounding the wheels of the cars. Again, red color indicates flow of greatest magnitude and blue color indicates flow of lower magnitude. Both cars are designed with exposed wheels, which produce great drag, because of broad turbulent wakes. The top of the wheel moves through the air and generates a force that drags the air in the opposite direction of the flow. This interaction causes an early separation and consequently a broad wake.

Another effect of the exposed wheels is an increased lift force. The contact to the ground prevents air from passing underneath the tire, the air flows over and around the wheel. This causes a pressure difference, which leads to an upward force. This explains the red region at the top of the wheels in the figure. (Barnard, 2009)

The flow on the sides of the wheel also has a great impact of the generated drag, since the width of the wheel is usually small in comparison with the diameter.

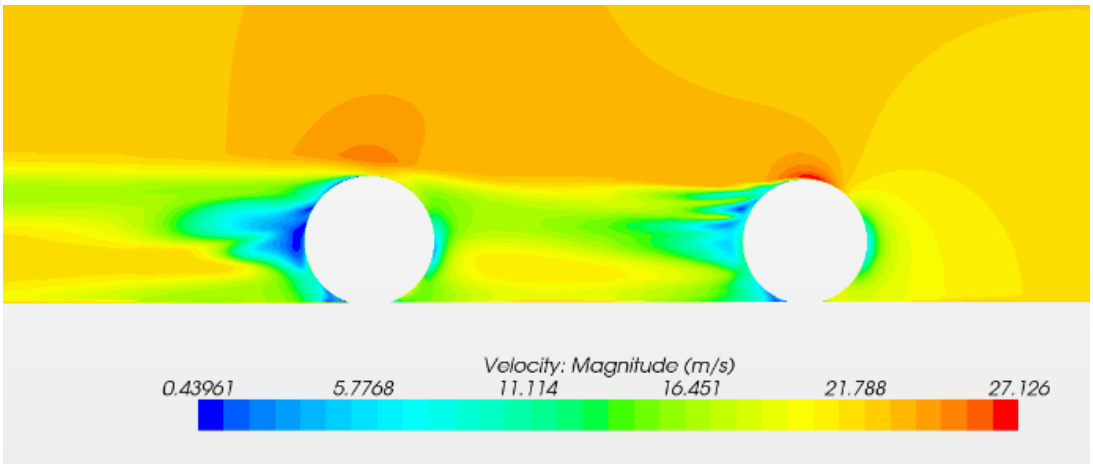

Figure 0-5: Cross-section showing the velocity of flow around the wheels of the Mercedes.

The front wheels of the Mercedes gives “shelter” to the rear wheels, since these are placed closer to the body and have a closed suspension. The flow around the rear wheels has a lower velocity than on the Auto Union. The wing shaped suspension covers accelerates the flow between the wheels and the car body this gives rise to a stream shaped flow and a lower pressure area along the car body, which can be noted in both figure 5-2 and 5-6. This reduces the pressure differences on the front and the back of the rear wheels and causes a reduction of drag on the rear wheels.

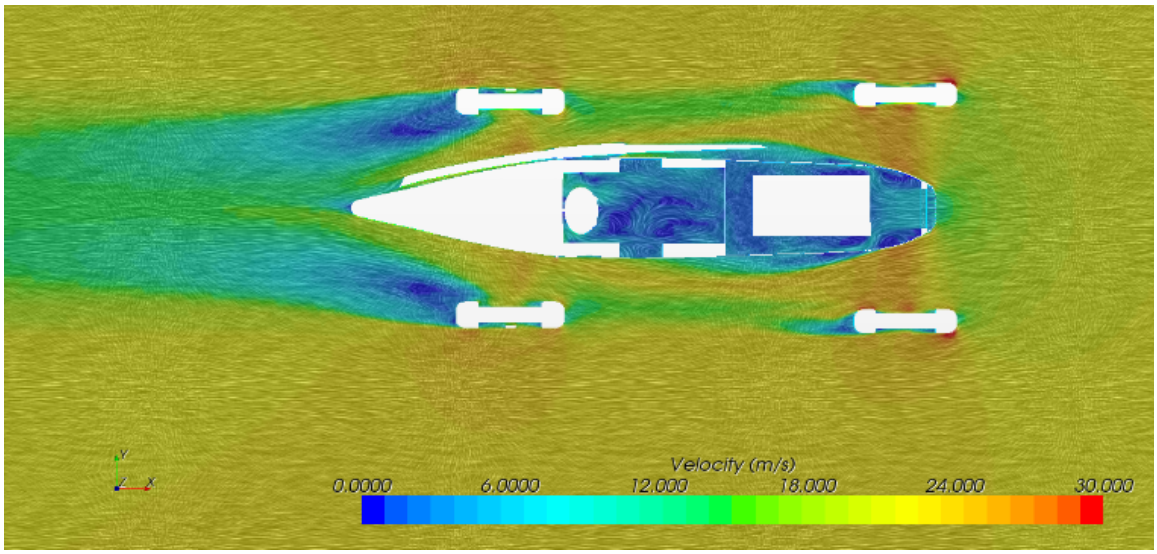

Figure 0-6: Vector velocity field of the Mercedes-Benz.

The Auto Union on the other hand, has a wider rear axle, which gives a greater frontal area and hence, a greater contribution to the total drag generated by the wheels. In figure 5-7 below it can be noted that the velocity of the flow around the rear wheels on the Auto Union is of higher magnitude then on the Mercedes. Due to the exposed suspension on the wheels the flow acts more turbulent around the front wheels which contribute to a more irregular flow pattern.

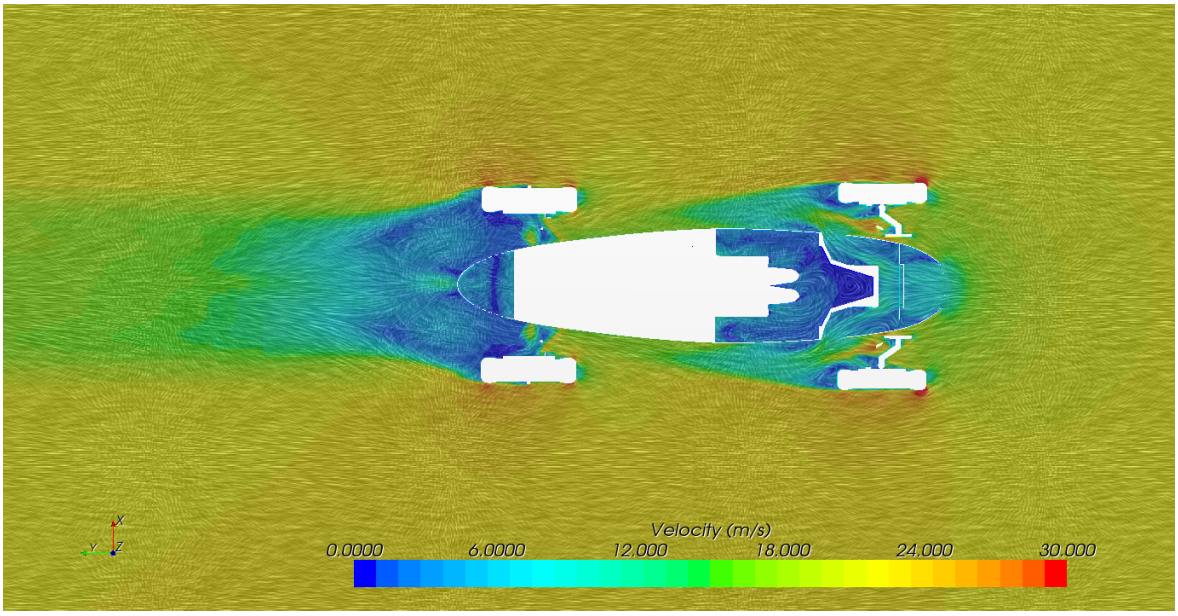

Figure 0-7: Vector velocity field of the Auto Union.

Discussion

In this section the method and results of the project is discussed.

1.22 Method

The approach used for this project is a standard CFD analysis method, using CAD models and commercial CFD software. To produce the equivalent work and results with another method would have been hard to achieve.

1.22.1 Pre processing

The construction part of the project, making the CAD-models, went as planned. Even though minor problems arose along the way, milestones were always reached in time. The group was rather familiar with the software used for this part, CATIA v5, which led to an efficient progress. The parts unknown were easily learned through tutorials. When preparations for an optimal mesh were to begin, so did usage of unfamiliar software, ANSA and STAR CCM+. Here, more thorough studies of tutorials were required, and reduced the gap between knowledge of the group and knowledge needed. Nevertheless, the supervisors had to fill in from time to time. A couple of time-consuming, but educational mistakes were made, but overall the group met the expectations and produced representative CAD models and volume meshes, ready for simulations.

1.22.2 Solving

This part was also done in STAR CCM+ and as above the inexperience of the software was limiting, causing further tutorial studies. Also, it led to a lot of discussions with the supervisors regarding the set up for the simulations and with their help most of the settings were made. This, together with several iterations of solving and resetting, resulted in satisfactory simulations.

1.22.3 Post Processing

The post processing was a bit undermined because the project was emphasized on the pre processing. A different allocation of time for the different parts of the project could have been rewarding for the analysis of the results. On the other hand, if the time for pre processing would have been reduced, the quality of the CAD models would likely have decreased which would have led to less accurate simulations.

1.23 Mesh validation

Considering the time constraint and computer power available for this project the mesh size was limited to consist of a maximum of 10-15 million cells. For the level of accuracy in this analysis the results are considered fairly accurate hence a finer mesh would not change the result in a radical way. However, if the project were to analyze the cars on a more detailed level, calculations with a finer mesh would have been appropriate.

To get a good representation near the wall, three prism layers were applied to the geometry. The choice to have three layers was based on two things: first, the fact that fewer amounts of layers would not give a good enough representation of the geometry, and second, more layers would demand too much computational power, because of the great increase of cells.

1.24 Sources of errors

Even though the simulations produced realistic and acceptable results, some sources of errors are necessary to discuss:

The CAD models, compared to the real cars, are simplified. Interiorly, the geometry of the engine and other parts has been either neglected or very constrained. Exteriorly, minor details were ignored and the underbody was strictly generalized. The flow through the car is simplified, both geometrically because of the generalization of the internal parts and because of the neglected thermal impact. The method used to construct the shape of the body, extracting contours from the scan data and measuring the CMC-models, resulted in good surfaces. However, capturing the exact shapes using this method is difficult, hence this may cause some inaccurate flow behavior.

The $k - \varepsilon$ turbulence model were chosen for both its accuracy and its relatively low computer power demand. Models exist where the Reynolds stresses are modeled directly instead of reducing all the effects of turbulent eddies to a turbulent viscosity term. Unfortunately they demand a lot of computational power; therefor they were never an option for this project.

The equations solved in the calculation were solved iteratively as a steady state and not as transient. This means that the resulting simulation does not show fluctuation in the flow, instead a time-averaged result can bee seen. A slight difference can be expected regarding drag force comparative to a transient solution but the gain in computational power required annuls this issue.

Some problems occurred in the computations of the Auto Union, which were exposed by the residuals not converging. After a number of resets and recalculations a satisfying solution was received. The residuals had still not converged as much as ideal, but enough to claim the simulation was successful. The reason for why these problems occurred was never identified. Conclusion can be drawn that the problem was not leaving a discoverable impact hence was not that important for the results.

1.25 In conclusion

The simulations show that the Silver Arrows are rather well shaped from aerodynamic perspective; however, the design includes some drag-producing features. In total, the Mercedes-Benz performed better than the Auto Union, producing less drag force and more downforce.

The aerodynamic properties of the car are assumed to be affected by the sources of error in various ways. For example the lack of detail of the underbody which has lead to a smoother model than the real car’s and hence a less obstructed flow under the model. To get an even greater understanding of the aerodynamic properties of the vehicles a more comprehensive analysis would be necessary, including both a fully detailed CAD model and the thermodynamics effects.

Overall, the group is content with the result of the project and considers the objectives to be fulfilled. However, because of the emphasis on the pre processing, some planned parts of the project were cut off. Originally, the CFD simulations were to be done in two different velocities. Also, wind tunnel testing of the CMC-models was to be compared with the resulting simulations. These parts would have contributed to the project a broader analysis of the Silver Arrows, why the project group recommends further tests and simulations, including above described cases.

Bibliography

Barnard, R. (2009). *Road Vehicle Aerodynamic Design: An introduction.*

Batchelor, G. K. (2000). *Intoduction to Fluid Dynamics.* New York: Cambridge University Press.

Becker, C. (2002). *Mercedes-Benz Silver Arrows.*

David, D. (1999). *Grand Prix History.* Retrieved 2013-12-03 from http://www.grandprixhistory.org/

Finite Volume. (2012). Retrieved 2013-16-05 from CFD Online: http://www.cfd-online.com/Wiki/Finite_volume

FLUENT. (2003). *FLUENT 6.1 User's Guide* (January, 2003 ed.).

Hansen, G. A. (2005). *Mesh Enhancement : Selected Elipptic Methods, Fondations and Applications.* London: Imperial College Press.

Kirchberg, P. (2008). *Bernd Rosemeyer.*

M.White, F. (2011). *Fluid Mechanics.*

McBeath, S. (2008). *Competition Car Aerodynamics.*

Snellman, L. (2012). Retrieved 2013-13-03 from http://www.kolumbus.fi/leif.snellman/c9.htm

Sovran, D. V. (1996). *Vehicle Aerodynamics.*

Appendix A

CAD parts of Mercedes-Benz W25

Side mirror & windshield

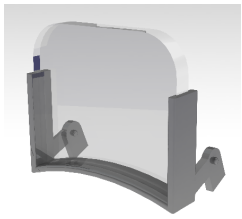

Wheel & wheel suspension

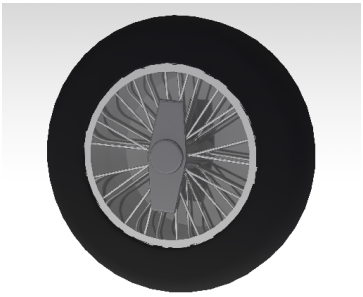

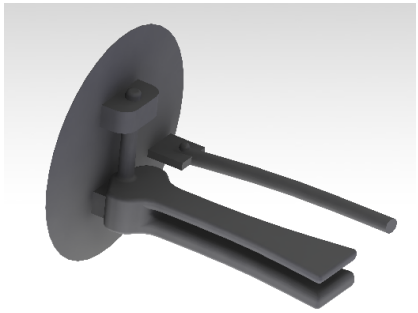

Engine cover pin & air intake

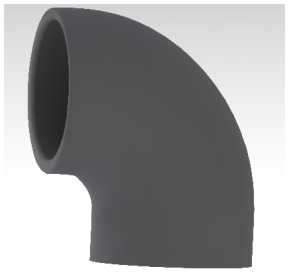

Steering wheel & exhaust pipe

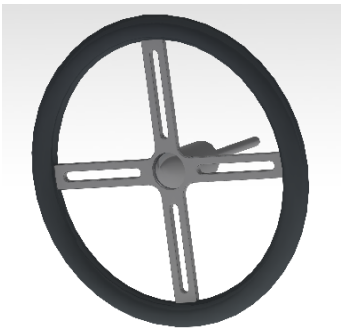

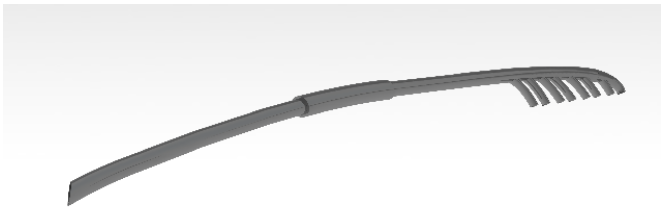

CAD parts of Auto-Union Type C

Wheel & wheel suspension

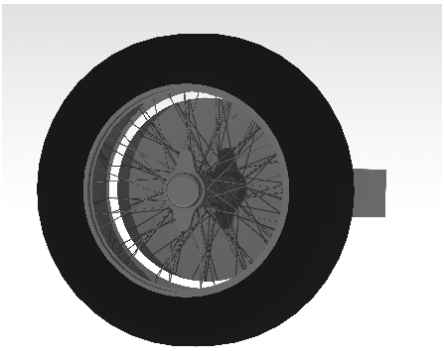

Side mirror & air intake

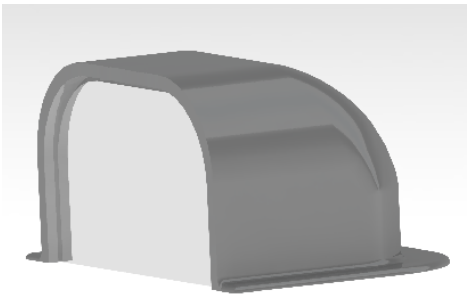

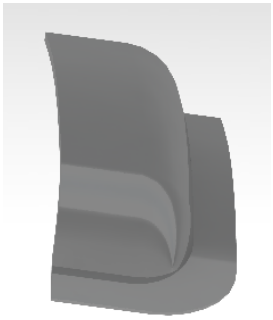

Steering wheel & windshield

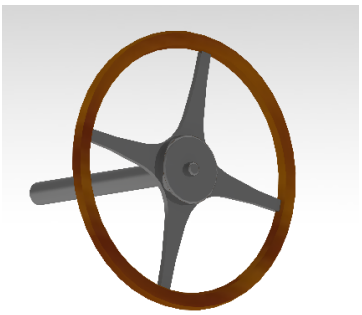

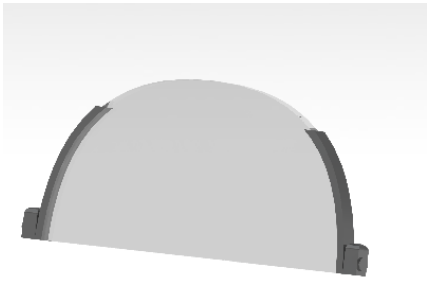

Engine cover buckle & front grill

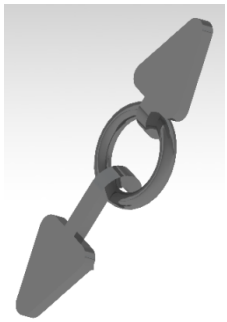

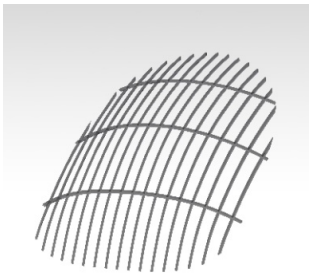

Air intake & exhaust pipe

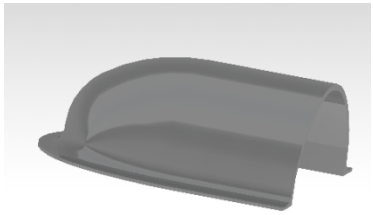

Transmission detail & pipe

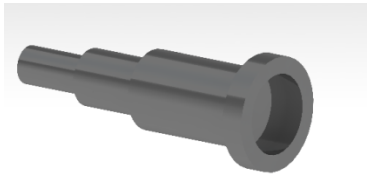

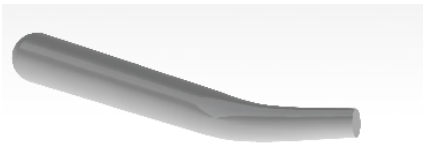

Gas cup & radiator cup

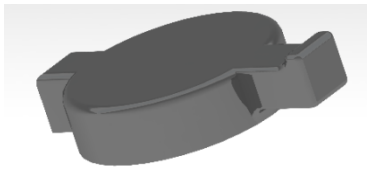

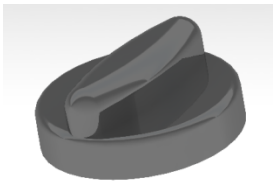

Seat & helmet with goggles

Appendix B

Values for different PIDs:

Mercedes-Benz W25:

Details include: pins, hose, windscreen, steering-wheel,
exhaust pipe, side mirror, wheel suspension

Part	Min (mm)	Target (mm)
Grills	2	4
Goggles	4	8
Cooler Wall	4	8
Cooler inlet	4	8
Cooler outlet	4	8
Cooler sides	4	8
Wheels	4	8
Wings	4	8
Helmet	4	8
Details	4	8
Body upper	4	8
Outer surface	8	16
Body lower	8	16
Seat	8	16
Inner surface	14	16
Engine room	14	16

Auto-Union Type C:

Part	Min (mm)	Target (mm)
Vents	2	4
External parts	4	8
Goggles	4	8
Suspension	4	8
Wheel front	4	8
Wheel rear	4	8
Radiator in	4	8
Radiator out	4	8
Radiator sides	4	8
Driver top	4	8
Helmet	4	8
Internal cockpit	8	16
Body	8	16
Internal body	14	16

External parts include:
Wind shield
Mirrors
Rear hose
Front hose
Engine belts
Transmission tail
Steering wheel
Air inlet rear
Air inlet front
Water cap
Fuel cap
Exhaust